Water and nitrogen dynamics in soybeans: integration of crop modeling and field data

by

Gabriel da Rocha Hintz

B.S., Federal University of Santa Maria, 2023

A THESIS

submitted in partial fulfillment of the requirements for the degree

MASTER OF SCIENCE

Department of Agronomy
College of Agriculture

KANSAS STATE UNIVERSITY
Manhattan, Kansas

2024

Approved by:

Major Professor
Dr. Ignacio A. Ciampitti

Copyright

© Gabriel da Rocha Hintz 2024.

Abstract

Soybeans [*Glycine max* (L.) Merr.] are a vital component of global agriculture, providing a major source of protein, oil, and animal fodder. Global production has increased significantly in recent decades, with Brazil, the United States, and Argentina collectively accounting for 80% of global soybean production. However, 60-70% of the soybean cropland area is grown under rainfed conditions, rendering yields particularly vulnerable to climate variability. Particularly, the variability in rainfall can account for up to 60% of yield variations in key agricultural regions. Moreover, soybean production requires substantial nitrogen (N) inputs, with approximately 80 kg of N needed per Mg of seed produced. Soybeans satisfy this N demand from both soil and symbiotic N fixation processes, making it essential to isolate those sources for investigating this nutrient dynamics. This study had two principal objectives. First, Chapter 2 aimed to characterize water stress (WS) patterns during El Nino Southern Oscillation (ENSO) events and assess the impact of climate-adaptive management strategies— particularly the timing of planting and the selection of maturity group (MG), on the mitigation of yield loss and the optimization of soybean seed yield in Southern Brazil. Second, Chapter 3 aimed to review current knowledge on N dilution curves for soybeans to establish a baseline model, define a critical N dilution curve using non-nodulating genotypes, and investigate the physiological mechanisms underlying the relationship between plant growth and N sources. For the first objective, Chapter 2, crop growth simulations were performed using Agricultural Production Systems Simulator (APSIM) Next-Generation to test three soybean MGs (5.0, 5.8, and 6.4) across eight planting dates (from October 5th to January 20th) over 30 years at 187 locations in Rio Grande do Sul (RS), Brazil. The risk of crop failure was calculated as the percentage of simulations yielding less than the economic break-even yield threshold for soybean production.

The simulated yields were grouped into four regions: Northeast (NE), North (N), Central (C), and Southwest (SW). The WS patterns were classified into four categories: no stress, early stress, late stress, and whole season stress. On average, the application of water stress (WS) resulted in a reduction in yield of up to 2 Mg ha^{-1}, which represents a decrease of approximately 50% relative to the yield obtained under conditions of no stress. The frequency and severity of WS patterns varied across regions, with the SW experiencing more frequent and severe stress, including up to 50% of whole season stress during La Nina events. ENSO events influenced WS frequency, with El Niño events associated with reduced stress and La Niña events correlating with increased stress. The MG 5.0 resulted in the highest probability of failure in all regions, and early planting dates showed the greatest yield variability (up to 5 Mg ha^{-1}). For the second objective, Chapter 3, a literature review was conducted to compile data on N dilution curves for soybeans. Additionally, a field experiment was conducted in Kansas, United States, using four soybean genotypes (two nodulating and two non-nodulating) under four fertilizer N rates (0, 100, 200, and 300 kg N ha^{-1}). Non-nodulating soybeans exhibited a 46% greater N dilution compared to their nodulating counterparts. Nodulating genotypes reported greater specific leaf area (20%) and specific leaf nitrogen (45%), with a reduction in the specific leaf weight (17%). The intrinsic N capacity increased not only for the leaf organ but in a similar proportion in stem and pod tissues, all acting as N reservoirs to meet seed N demand. Soil-%Nc followed a typical dilution pattern with increasing biomass, while atmospheric-%Nc increased during growth. In conclusion, the implementation of climate-adaptive strategies, including the optimization of planting dates and MGs, has demonstrated a 15% reduction in the risk of crop failure, thereby providing invaluable insights for enhancing the stability of soybean yields and the resilience of agricultural systems to the uncertainties posed by climate change. Furthermore, a pivotal crop N

dilution curve has been established for non-nodulating soybeans, exhibiting a greater degree of dilution than has been previously documented for nodulating varieties and presenting new evidence of N allocation within this crop.

Table of Contents

List of Figures viii
List of Tables xi
Acknowledgements xii
Dedication xiii
Chapter 1 - General Introduction 1
References 3
Chapter 2 - Climate-adaptative Management Strategies for Soybean Production under ENSO Scenarios in Southern Brazil: An in-silico Analysis of Crop Failure Risk 5
Abstract 5
Introduction 6
Methods 9
Study region description 9
Model parametrization and validation 9
Model inputs for long-term simulations 11
Results 15
Model validation 15
Spatial clustering, water stress, environmental type classification, and soybean yield dynamics 18
Water stress and ENSO frequency 19
Climate-adaptative management strategies 20
Crop failure risk 21
Discussion 23
Conclusions 26
Acknowledgements 27
References 27
Chapter 3 - Soybean Critical N Dilution Curve Using Non-nodulating Genotypes 35
Under review in Plant and Soil Journal. 35
Abstract 35
Introduction 36

Methods 37
Review on soybean plant N dilution curve 37
Field experiment 37
Experimental design and growing conditions 37
Field measurements and laboratory analyses 39
Statistical analysis 40
Critical N dilution curve 40
N uptake, leaf area, leaf weight, biomass and N concentration 42
Results 43
Review: soybean N dilution curves 43
Dynamics of plant N distribution and N sources 46
Discussion 48
Conclusions 51
References 51
Chapter 4 - Limitations and Future Fesearch 55
Appendix A - Chapter 2 57
Appendix B - Chapter 3 63

List of Figures

Figure 2.1. Workflow diagram highlighting the data collection before crop modeling investigation (Step 1), crop modeling structure (Step 2), characterization of water stress patterns and regions linked to ENSO phases (Step 3), and assessment of failure risk and development of climate-adaptative management strategies to counteract climate-driven yield penalties (Step 4). 15

Figure 2.2. In-season weather characterization (A) and model validation (B, C, D). Vertical dashed lines in A correspond to the in-season median precipitation and mean temperature, respectively. In B, C and D, circles, squares, and triangles represent MGs 5.0, 5.8 and 6.4, respectively. Red, blue, green, and purple correspond to the weather types cold and dry, cold and wet, hot and dry, and hot and wet, respectively. In-silico results obtained using APSIM crop growth model. 17

Figure 2.3. Soybean water stress patterns, clustered regions, and yield response: (A) water stress patterns. The relationship between water stress factor and crop development (thermal time). The vertical dashed line represents the early grain-filling phenological stage; (B) the distribution of soybean yield under varying water stress conditions in the four regions: Central (C), North (N), Northeast (NE), and Southwest (SW). The box plots illustrate the yield variability. The pie charts on the map, varying in color and size, represent the relative frequency of four categorized water stress patterns: no stress (green), early stress (purple), late stress (orange), and whole season stress (red) within each region; (C) distribution of soybean yields across the Southwest (SW), Central (C), North (N), and Northeast (NE) regions. In-silico results obtained using APSIM crop growth model. 19

Figure 2.4. Frequency of water stress patterns across four regions during La Niña, Neutral, and El Niño phases. The heatmap conveys the percentage of stress occurrences, with color intensity indicating frequency. In-silico results obtained using APSIM crop growth model. 20

Figure 2.5. Cumulative frequency of yield across regions (columns), ENSO (rows), maturity groups (linetype), and planting dates (colors). Yield is expressed as the difference with the average of each region. In-silico results obtained using APSIM crop growth model. 21

Figure 2.6. Comparative descriptive analysis of crop failure risk across different ENSO phases (colors): (A) Probability density functions for the four regions (panels) showing risk distribution under El Niño, Neutral, and La Niña conditions; (B) Percentage of crop failure associated with maturity groups (MGs) in each region; (C) Percentage of crop failure linked to planting dates. In-silico results obtained using APSIM crop growth model. 23

Figure 3.1. Synthesis-analysis of plant N dilution curves for soybeans (A). Relationship between plant N concentration (%Nc) and plant biomass for nodulating (Nod) and non-nodulating (Non-nod) genotypes (B). In B, the red line corresponds to the critical N dilution curve (%N = 4.9 $W^{-0.26}$) adjusted for nodulating genotypes, while the blue line corresponds to the critical N dilution curve adjusted for non-nodulating genotypes (% N = 5.0 $W^{-0.38}$). Those critical dilution curves were established using the data of all fertilizer N rates, following the guidelines provided by Fernandez et al. (2022). The shaded area corresponds to the 95% credible interval..... 45

Figure 3.2. Plant nitrogen uptake as a function of aboveground plant biomass (A) for nodulating (Nod) and non-nodulating (Non-nod) genotypes, with nodulating genotypes described by y = $0.757x^{0.68}$ and non-nodulating genotypes by y = $0.757x^{0.52}$. Nitrogen uptake on leaves versus leaf area (B) reveals a linear increase that can be described by y = 0.016x and y = 0.011x for nodulating (nod) and non-nodulating (non-nod) genotypes, respectively. Leaf weight relative to leaf area (C) for nodulating (nod, y = 0.311x) and non-nodulating (non-nod, y = 0.375x) genotypes. Relationship of N uptake (g plant-1) by pods and pods biomass (g $plant^{-1}$) (D) for nodulating (red) and non-nodulating genotypes (blue). Nodulating are described by y = 0.04x, and non-nodulating are described by y = 0.025x. 47

Figure 3.3. Variations in N source utilization across plant biomass levels. The relationship between plant N concentration derived from soil N sources (soil-%Nc, %) and plant biomass (g $plant^{-1}$) (A) can be described by y = $6.4564x^{-0.3418}$ for the nodulating genotype and by y = $6.4564x^{-0.4283}$ for the non-nodulating genotype. The relationship between plant N concentration derived from the N fixation process (atmospheric-N, %Nc, %) and plant biomass (A) can be described by y = $0.07x^{0.58}$ for the nodulating genotype. Plant N uptake sourced from soil (circles– solid line) and atmosphere (triangles – dashed line) (C) are described by y = $0.1030x^{0.52}$ and y = $0.0015x^{1.35}$. Red symbols and lines correspond to nodulating, and blue corresponds to non-nodulating genotypes..... 48

Appendix Figure A.1. Comparison of observed weather data (INMET – National Meteorology Institute) and gridded weather data (CHIRPS). The bottom panel illustrates an example of the soybean simulated grain yield utilizing observed (solid lines) and gridded (dashed lines) weather data in contrasting seasons. 61
Appendix Figure A.2. Sites utilized for validation (circles) and calibration (triangles). Colors indicate the Relative Root Mean Square Error (RRMSE), and circle size indicates the number of observations at each validation site. 61
Appendix Figure A.3. Sensitivity analysis of economic break-even yield impact on crop failure risk (%). Quantiles q25 = 1.5 Mg ha^{-1}, median = 2.0 Mg ha^{-1}, and q75 = 2.6 Mg ha^{-1}. 62
Appendix Figure B.1. In-season weather characterization: maximum (red) and minimum (blue) temperatures, and precipitation (black bars). Sampling times, sowing, and harvest are illustrated..... 63
Appendix Figure B.2. Comparison of non-nodulating genotypes under no N limitation (300 kg N) curve (black) with the curves presented in Figure 3.1. 64
Appendix Figure B.3. The relationship between plant aboveground biomass and leaf/stem N ratio was the same for both genotypes and can be described by $y = 2.5575 - 0.0332x$. Red symbols and lines correspond to nodulating genotypes, blue symbols and lines correspond to non-nodulating genotypes. 65

List of Tables

Table 2.1. Model validation metrics across maturity groups and weather types. Root mean square error (RMSE) and relative root mean square error for days to flowering, days to maturity and yield. 16

Table 3.1. Reported parameters for soybean N dilution curves in previous studies (adapted from Santachiara et al., 2018). The A1 parameter refers to plant N concentration at 1 Mg ha^{-1}, and the A2 parameter regulates the intensity of the plant N dilution over time. 43

Table 3.2. Soybean seed yield, biomass (Mg ha^{-1}) and plant N concentration (%Nc) at varying crop growth stages for all genotypes under different fertilizer N rates. 44

Appendix Table A.1. Validation dataset description. 57

Appendix Table A.2. APSIM Next Generation phenology parameters. 58

Appendix Table B.1. Experiment soil characterization. 65

Acknowledgements

The creation of this document and the personal-professional achievements it represents would not have been possible without the support of many individuals along the way.

First and foremost, I extend my heartfelt gratitude to my parents, Jaques and Andrea, who spared no effort in providing me with a quality education. To my brother, Arthur, that together with my parents, overcame the long distance to support me. To Claire, for all the partnership and support during good and hard moments.

To all members of Ciampitti Lab from 2022 to 2024, especially Dennis and the field team in 2022 that made me feel at home, even thousands of miles away from home in my first experience abroad. That year brought me friends I will remember forever. Also, thanks to all students and post-docs that empowered my knowledge though discussions and knowledge sharing. Luiz, I would not have made it without all the hours you dedicated to teaching me statistics and programming.

Ignacio, your guidance and leadership have been truly inspiring. Your support, dedication, and availability to your students are a gift to our professional careers. Thank you for all the opportunities and mentorship. I also extend my gratitude to my committee members, Dr. Prasad and Dr. Hefley, for their guidance and direction throughout my MSc program.

Dedication

I dedicate this thesis to my family, whose unwavering support and encouragement have been my guiding light. Their boundless efforts and sacrifices have made this journey possible. Thank you for believing in me and for being my constant source of strength and inspiration.

Chapter 1 - General Introduction

Soybeans (*Glycine max* (L.) Merr.) represent a cornerstone of global agriculture, providing a vital source of protein, oil, and fodder (Duan et al., 2023; Wang et al., 2020). Over the past three decades, global soybean production has increased by approximately 9 Tg per year, with Brazil, the United States, and Argentina collectively accounting for 80% of total production in 2022 (FAO, 2024). However, despite these production gains, it is notable that nearly 60-70% of the world's crop production is grown under rainfed conditions (Rost et al., 2009), with only 15% of the soybean cultivated area benefiting from irrigation (Rosegrant et al., 2002).

The reliance on rainfed agriculture makes soybean yields highly sensitive to climate variability, which can cause up to 60% of the observed yield variability in key agricultural regions (Ray et al., 2015). Global climate variability alone accounts for about one-third of all yield fluctuations (Ray et al., 2015). Furthermore, it has been estimated that global production could be increased by 19% with the implementation of improved water management practices (Rost et al., 2009). This highlights the critical need for developing climate-adaptive management strategies, including planting dates and the selection of appropriate maturity groups, to stabilize yields (Kukal and Irmak, 2018; Lobell et al., 2011; Mourtzinis et al., 2015; Rezaei et al., 2023). Yet, despite growing awareness of these challenges, research still lacks a clear understanding of how specific weather patterns influence soybean production, especially in relation to water availability and climate variability (Ray et al., 2015). Addressing these gaps is vital for ensuring food security, enhancing sustainability, and maintaining the profitability of modern agricultural systems (Brauman et al., 2013; Dubey et al., 2019).

In addition to the challenges posed by climate change, the production of high soybean yields necessitates substantial inputs of nitrogen (N), with an estimated 80 kg of N required for

each Mg of seed produced (Ciampitti and Salvagiotti, 2018). Nitrogen management is one of the most critical factors for optimizing crop yields, and its importance spans across various crops. In this context, the N dilution curve has been used as a diagnostic tool for N status in wheat (*Triticum aestivum* L.) (Justes et al., 1994), maize (*Zea mays* L.) (Plénet and Lemaire, 1999), and soybean (Divito et al., 2016). The critical N dilution curve defines the minimum plant N concentration (%Nc) required to maximize crop growth, with plant %Nc decreasing as the crop reaches maturity (Greenwood et al., 1990; Lemaire et al., 2008; Plénet and Lemaire, 1999). While several studies have reported nitrogen dilution curves for soybeans (Almeida et al., 2023; Divito et al., 2016; Ney et al., 1997; Salvagiotti et al., 2008; Santachiara et al., 2018). Furthermore, soybeans possess an additional N source via symbiotic relationships with microorganisms that fix atmospheric N. This ability complicates the development of a single, universally applicable critical N dilution curve, as both soil-derived and symbiotically fixed nitrogen must be considered. To accurately define this curve, it is essential to segregate these nitrogen sources, with non-nodulating isolines serving as a valuable tool in this quantification process.

This study was set up to investigate two aspects of soybean production with emphasis on water stress characterization and yield mitigation, and the N dilution curve and physiological mechanisms related to the crop N nutrition in soybeans. In Chapter 2, the main objectives were to: i) characterize water stress and spatial patterns and their frequency within ENSO events; and ii) explore the impact of two strategic climate-adaptative management strategies - planting date and maturity group - associated with ENSO events in mitigating crop failure risk and maximizing seed yield in Southern Brazil. In Chapter 3, the main objectives were to: i) conduct a review to provide a synthesis of the current knowledge on N dilution curves for soybeans; ii)

define a critical N dilution curve using non-nodulating soybean genotypes; and iii) study the main physiological mechanisms governing the relationship between plant growth and N sources (soil and atmosphere) for this crop. Lastly, Chapter 4, presents a summary and provides new insights on the main limitation and future research steps.

References

A. Almeida, L.F., Correndo, A., Ross, J., Licht, M., Casteel, S., Singh, M., Naeve, S., Vann, R., Bais, J., Kandel, H., Lindsey, L., Conley, S., Kleinjan, J., Kovács, P., Dan Berning, Hefley, T., Reiter, M., Holshouser, D., Ciampitti, I.A., 2023. Soybean yield response to nitrogen and sulfur fertilization in the United States: contribution of soil N and N fixation processes. European Journal of Agronomy 145, 126791. https://doi.org/10.1016/j.eja.2023.126791

Brauman, K.A., Siebert, S., Foley, J.A., 2013. Improvements in crop water productivity increase water sustainability and food security—a global analysis. Environ. Res. Lett. 8, 024030. https://doi.org/10.1088/1748-9326/8/2/024030

Ciampitti, I.A., Salvagiotti, F., 2018. New Insights into Soybean Biological Nitrogen Fixation. Agronomy Journal 110, 1185–1196. https://doi.org/10.2134/agronj2017.06.0348

Divito, G.A., Echeverría, H.E., Andrade, F.H., Sadras, V.O., 2016. Soybean shows an attenuated nitrogen dilution curve irrespective of maturity group and sowing date. Field Crops Research 186, 1–9. https://doi.org/10.1016/j.fcr.2015.11.004

Duan, Z., Li, Q., Wang, H., He, X., Zhang, M., 2023. Genetic regulatory networks of soybean seed size, oil and protein contents. Frontiers in Plant Science 14.

Dubey, A., Kumar, A., Abd_Allah, E.F., Hashem, A., Khan, M.L., 2019. Growing more with less: Breeding and developing drought resilient soybean to improve food security. Ecological Indicators 105, 425–437. https://doi.org/10.1016/j.ecolind.2018.03.003

FAOSTAT [WWW Document], n.d. URL https://www.fao.org/faostat/en/#home (accessed 10.16.23).

GREENWOOD, D.J., LEMAIRE, G., GOSSE, G., CRUZ, P., DRAYCOTT, A., NEETESON, J.J., 1990. Decline in Percentage N of C3 and C4 Crops with Increasing Plant Mass. Annals of Botany 66, 425–436. https://doi.org/10.1093/oxfordjournals.aob.a088044

Justes, E., Mary, B., Meynard, J.-M., Machet, J.-M., Thelier-Huche, L., 1994. Determination of a Critical Nitrogen Dilution Curve for Winter Wheat Crops. Annals of Botany 74, 397–407. https://doi.org/10.1006/anbo.1994.1133

Kukal, M.S., Irmak, S., 2018. Climate-Driven Crop Yield and Yield Variability and Climate Change Impacts on the U.S. Great Plains Agricultural Production. Sci Rep 8, 3450. https://doi.org/10.1038/s41598-018-21848-2

Lemaire, G., Jeuffroy, M.-H., Gastal, F., 2008. Diagnosis tool for plant and crop N status in vegetative stage: Theory and practices for crop N management. European Journal of Agronomy 28, 614–624. https://doi.org/10.1016/j.eja.2008.01.005

Lobell, D.B., Schlenker, W., Costa-Roberts, J., 2011. Climate Trends and Global Crop Production Since 1980. Science 333, 616–620. https://doi.org/10.1126/science.1204531

Mourtzinis, S., Specht, J.E., Lindsey, L.E., Wiebold, W.J., Ross, J., Nafziger, E.D., Kandel, H.J., Mueller, N., Devillez, P.L., Arriaga, F.J., Conley, S.P., 2015. Climate-induced reduction in US-wide soybean yields underpinned by region- and in-season-specific responses. Nature Plants 1, 1–4. https://doi.org/10.1038/nplants.2014.26

Ney, B., Dore, T., Sagan, M., 1997. Grain Legumes, in: Lemaire, G. (Ed.), Diagnosis of the Nitrogen Status in Crops. Springer, Berlin, Heidelberg, pp. 107–117. https://doi.org/10.1007/978-3-642-60684-7_6

Plénet, D., Lemaire, G., 1999. Relationships between dynamics of nitrogen uptake and dry matter accumulation in maize crops. Determination of critical N concentration. Plant and Soil 216, 65–82. https://doi.org/10.1023/A:1004783431055

Ray, D.K., Gerber, J.S., MacDonald, G.K., West, P.C., 2015. Climate variation explains a third of global crop yield variability. Nat Commun 6, 5989. https://doi.org/10.1038/ncomms6989

Rezaei, E.E., Webber, H., Asseng, S., Boote, K., Durand, J.L., Ewert, F., Martre, P., MacCarthy, D.S., 2023. Climate change impacts on crop yields. Nat Rev Earth Environ 4, 831–846. https://doi.org/10.1038/s43017-023-00491-0

Rosegrant, M. W., Cai, X., Cline, S. A., & Nakagawa, N. (2002). The role of rainfed agriculture in the future of global food production.

Rost, S., Gerten, D., Hoff, H., Lucht, W., Falkenmark, M., Rockström, J., 2009. Global potential to increase crop production through water management in rainfed agriculture. Environ. Res. Lett. 4, 044002. https://doi.org/10.1088/1748-9326/4/4/044002

Salvagiotti, F., Cassman, K.G., Specht, J.E., Walters, D.T., Weiss, A., Dobermann, A., 2008. Nitrogen uptake, fixation and response to fertilizer N in soybeans: A review. Field Crops Research 108, 1–13. https://doi.org/10.1016/j.fcr.2008.03.001

Santachiara, G., Salvagiotti, F., Gerde, J.A., Rotundo, J.L., 2018. Does biological nitrogen fixation modify soybean nitrogen dilution curves? Field Crops Research 223, 171–178. https://doi.org/10.1016/j.fcr.2018.04.001

Wang, S., Liu, S., Wang, J., Yokosho, K., Zhou, B., Yu, Y.-C., Liu, Z., Frommer, W.B., Ma, J.F., Chen, L.-Q., Guan, Y., Shou, H., Tian, Z., 2020. Simultaneous changes in seed size, oil content and protein content driven by selection of SWEET homologues during soybean domestication. National Science Review 7, 1776–1786. https://doi.org/10.1093/nsr/nwaa110

Chapter 2 - Climate-adaptative Management Strategies for Soybean Production under ENSO Scenarios in Southern Brazil: An in-silico Analysis of Crop Failure Risk

Published in the Agricultural Systems Journal.

Hintz, G., Carcedo, A., Almeida, L. F., Corassa, G., Horbe, T., Pott, L., ... & Ciampitti, I. (2025). Climate-adaptative management strategies for soybean production under ENSO scenarios in Southern Brazil: An in-silico analysis of crop failure risk. Agricultural Systems, 222, 104153. https://doi.org/10.1016/j.agsy.2024.104153.

Abstract

Soybeans (*Glycine max* L.) are a crucial crop for global food security, and the state of Rio Grande do Sul (RS), Brazil, plays a significant role. However, climate instability, particularly water stress (WS), is a major concern in this region, causing large interannual yield variability. This study aims to address this issue using an in-silico approach to: i) characterize WS and spatial patterns and their frequency within ENSO events; and ii) explore climate-adaptative management strategies such as planting dates and maturity groups to mitigate the risk of crop failure and maximize seed yield and profits. Crop growth simulations were performed testing three soybean maturity groups (MG, 5.0, 5.8, and 6.4) and eight planting dates (from October 5th to January 20th) over 30 years at 187 locations in RS, Brazil, using APSIM Next Generation. Failure risk was calculated as the percentage of simulations that yielded less than the economic break-even soybean yield in a given scenario. The simulated yields were clustered into four regions: Northeast, North, Central, and Southwest. Four WS seasonal patterns were then defined (no stress, early stress, late stress, and whole season stress). On average, WS reduced yields up to

2 Mg ha-1 (~50% relative to the maximum). WS varied among regions, with the SW experiencing more frequent and severe stress (up to 50% of whole season stress during La Nina). ENSO events influenced WS frequency, with El Niño events associated with reduced stress and La Niña events to increased stress. The MG 5.0 resulted in a higher probability of failure risk in all regions. Early planting dates resulted in the highest yield variability (up to 5 Mg ha-1). Climate-adaptative management strategies, such as optimizing planting dates and maturity groups, resulted in a 15% reduction in crop failure. Our findings provide valuable insights for developing targeted approaches to enhance soybean yield stability, thereby increasing the resilience of agriculture in the face of future climate uncertainties.

Introduction

Soybeans (*Glycine max* (L.) Merr.) represent a cornerstone of global agriculture, serving as a vital source of protein, oil, and fodder (Duan et al., 2023; Wang et al., 2020). Brazil plays a critical role as the major soybean producer in the world (FAO, 2024). In this context, the state of Rio Grande do Sul (RS, located in the southern part of Brazil) is particularly noteworthy, contributing about 15% of the total soybean planted area in Brazil (CEPEA, 2024; CONAB, 2024). However, a major concern in RS is the large interannual yield variability, mainly attributed to climate instability (Sentelhas et al., 2015), which affects the economic stability of this crop. Rio Grande do Sul is especially vulnerable to water stress (WS), as the majority (~98%) of agricultural systems operate under dryland conditions (Martins et al., 2021). Therefore, seasonal variations in precipitation and temperature significantly impact soybean yields, highlighting the urgent need to develop climate-adaptative management strategies (Kukal and Irmak, 2018; Lobell et al., 2011; Mourtzinis et al., 2015; Rezaei et al., 2023), such as planting date and maturity group (MG). In this context, there is a clear research gap in

understanding the impact of weather patterns and their influence on soybean production (Ray et al., 2015).

For the southern region of Brazil, previous studies have focused on assessing the impact of the El Niño Southern Oscillation (ENSO) and including planting date as a relevant climate-adaptive mitigation practice (Cai et al., 2020; Nóia Júnior et al., 2020; Nóia Júnior and Sentelhas, 2019). The ENSO phases can be used to predict rainfall and temperature variation, ultimately impacting overall crop productivity (Iizumi et al., 2014; Ropelewski and Halpert, 1987). Therefore, it is critical to address the implications of water availability on food security, sustainability, and profitability of the current agricultural farming systems (Brauman et al., 2013; Dubey et al., 2019). WS as a critical abiotic stressor (associated with ENSO) leads to significant yield reductions in soybean (Cohen et al., 2021; Du et al., 2020; Dubey et al., 2019; Gebre and Earl, 2020), but the overall pattern (timing and duration within the cropping season) remains to be investigated. Therefore, exploring climate-adaptative management strategies beyond planting date is key for developing more resilient agricultural farming systems.

The utilization of mechanistic crop growth models, such as the Agricultural Production Systems sIMulator (APSIM; Holzworth et al., 2014), have been employed to optimize soybean management strategies under different environmental conditions (Basche et al., 2016; Battisti et al., 2018; van Versendaal et al., 2023; Videla-Mensegue et al., 2021). Particularly in Brazil, numerous studies have documented the adaptation of crop management practices to prevailing environmental conditions, employing crop modeling as a foundational tool for assisting the farming decision-making process (Battisti et al., 2017, 2020b; Battisti and Sentelhas, 2019; Figueiredo Moura da Silva et al., 2021; Peterson et al., 2020). These models provide valuable insights on planting date and genetics adjustments, thereby enhancing crop resilience to climatic

stresses (Battisti et al., 2020a, 2018; Boote et al., 1996). Furthermore, crop models have been employed to comprehensively assess the interaction between planting date and ENSO phases and its impacts on yield variability and crop failure in the US (Perondi et al., 2023, 2022). Figueiredo Moura da Silva et al. (2021) have addressed the effect of maturity group factor but considering effect on future climate conditions. In addition, Battisti and Sentelhas (2019) developed environmental zones based on water deficits for soybeans, dividing RS in two regions (north and south) based on sowing date and soil types. However, to the extent of our knowledge, limited efforts have been made to quantify crop seasonal WS and spatial patterns (using hundreds of locations) to explore climate-adaptative management strategies beyond planting date. Considering the wide range of MGs used in RS and their significant interactions with planting date and environmental conditions, changes in crop growth cycle, assessing different soybean MGs, is a key climate-adaptative strategy that needs to be evaluated within the context of different ENSO events.

Following this rationale, this study employed APSIM crop growth model to develop an in-silico approach to test different climate-adaptative strategies for soybean crop under a broad range of environmental scenarios using two independent datasets in RS, Brazil. The specific objectives of this study implementing an in-silico approach were to: i) characterize WS and spatial patterns and their frequency within ENSO events; and ii) explore the impact of two strategic climate-adaptative management strategies such as planting dates and MGs associated with ENSO events in mitigating crop failure risk and maximizing seed yield.

Methods

Study region description

The study region encompasses the entire RS state (27º to 34º S and 50º to 58º W) in Southern Brazil. This region is characterized by a humid subtropical climate with hot and temperate summers (Alvares et al., 2013). The soils predominantly consist of Oxisols, Alfisols, Mollisols, Ultisols, Entisols and Inceptisols (Santos et al., 2018). Rio Grande do Sul is the second largest soybean producer state, dedicating ~6.7 millions of hectares, 63% of its cropland, to soybean cultivation in the 2023/2024 season (IBGE, 2024), with ~98% of the cropland managed under rainfed conditions (ANA, 2023; Martins et al., 2021).

Model parametrization and validation

The Agricultural Production Systems Simulator (APSIM) Next-Generation (Holzworth et al., 2014) was employed in this study, a modular model designed to explore agricultural landscapes (Brown et al., 2014). We used the soybean crop model for crop phenology, thermal time, and grain yield (Keating et al., 2003), SOILWAT for soil water content (Probert et al., 1998), Surface Organic Matter for residue management (Probert et al., 2004; Thorburn et al., 2001), and management rules for planting. Detailed information about the APSIM-Soybean model are available at https://builds.apsim.info/api/nextgen/docs/Soybean.pdf (last visited: April 2024).

The model was calibrated using field experiments conducted during the 2019/2020 and 2020/2021 growing seasons in Santa Rosa (54.44 °W 27.84 °S) and Cruz Alta (53.67 °W 28.60 °S), RS, Brazil (**Appendix Table A.1**). These experiments were part of the research efforts by the Cooperativa Central Gaucha Ltda. (CCGL). Three commercial soybean genotypes, BMX Raio IPRO, BMX Lanca IPRO, and BMX Fibra IPRO from Grupo Don Mario® (GDM),

representing the MGs 5.0, 5.8, and 6.4, respectively, were cultivated. These MGs are representative of those adopted by local farmers (Zanon et al., 2016).

The experimental design was a randomized complete block with five replications. Each plot consisted of five rows, 6 meters in length, spaced 0.5 meters apart. Seeds were inoculated with *Bradyrhizobium* sp. and sown at the recommended densities for each genotype. Crop phenology was monitored weekly from emergence to harvest, with five plants observed per sampling date. Seed yield was determined using a *Wintersteiger* plot harvester on the three central rows, accounting for 9 m^{-2}.

The APSIM model was calibrated for the three genotypes (Raio IPRO, BMX Lanca IPRO, and BMX Fibra IPRO). In APSIM, the phenological development is modeled as the progression through a sequence of developmental phases, each defined by a specific growth stage, with parameters quantifying crop growth duration and maturity (see calibrated parameters in **Appendix Table A.2**). The weekly crop phenology observations were converted to the APSIM phenology scale and parameterized using the Nelder-Mead optimization algorithm (Nelder and Mead, 1965; Wallach et al., 2018) within the *apsimx* (Miguez, 2024) package in R (R Core Team, 2024) (**See Appendix Table A.2**).

The model validation used an independent public data from Fundação Pró-Sementes (FPS) (available on *fundacaoprosementes.com.br*), for 13 locations within RS, spanning the 2013/2014 to 2020/2021 seasons. Planting dates varied from September 25th to January 20th, resulting in 4461 combinations of location, planting date, genotype, and season. The experimental design was a randomized block design with three repetitions. However, only the mean values of each treatment are provided and hence retrieved from the website. Plots consisted of five rows, four meters length and spaced 0.45 meters apart. Various seeding densities were

used according to the regional practices, using a pneumatic system planter. Seeds were treated with recommended insecticides and fungicides for soybean cultivation. Fertilization at planting was based on soil analysis. Seeds were inoculated with *Bradyrizobium japonicum* in the furrow at sowing. Insect and disease control during crop development followed Ministry of Agriculture of Brazil recommendations, with the number of applications varying by pest and disease occurrence. With a *Wintersteiger* plot harvester, yield was evaluated in the three central rows, totaling an area of 5.4 m^{-2}, with adjustments made for moisture content to 13%. Based on crop cycle, genotypes were grouped by MG to match the reference genotypes used in the calibration (MG ≤ 5.3 for BMX Raio IPRO (MG 5.0), MG 5.3 to 6.0 for BMX Lanca IPRO (MG 5.8), and MG > 6.0 for BMX Fibra IPRO (MG 6.4)).

Model performance was assessed through root mean square error (RMSE) and relative root mean square error (RRMSE). For both metrics, lower values indicate better performance.

Model inputs for long-term simulations

Simulations covered the three calibrated soybean genotypes across eight planting dates (October 5th to January 20th, in 15-day intervals), according to the typical sowing window for the studied region (CONAB, 2024). The study area was represented by a grid of 200 points equally spaced to capture environmental variability. We removed 13 locations lacking soil or weather information, resulting in 187 grid points spaced 39 km in longitude and 33 km in latitude, sufficient to capture the variability imposed by the weather and soil inputs. Simulations used a sowing density of 30 plants m^{-2}.For easiness of computation, gridded weather and soil data were employed. Daily precipitation was downloaded from CHIRPS (Funk et al., 2015), maximum and minimum temperature, and radiation were downloaded from NASAPOWER, and soil data was retrieved from and SoilGrids (“ISRIC — World Soil Information”; Poggio et al., 2021; Turek et

al., 2023). We chose CHIRPS over NASAPOWER for precipitation data, given its superior resolution. Comparisons of gridded and observed precipitation are present in **Appendix Figure A.1.** See Pott et al. (2022) for data validation using NASAPOWER and SoilGrids sources. At the start of the simulations, wheat residue (4 Mg ha-1) was added as soil cover, reflecting the widespread adoption of no-till farming in the region (CONAB, 2024; Fuentes-Llanillo et al., 2021).

The model was set to simulate daily WS, accumulated thermal time, phenology, and seed yield. WS was an output index from the crop growth model, calculated as the ratio between the total available plant soil water content and crop transpiration demand (Robertson et al., 2002). The WS factor was averaged for every 100 °Cd of thermal time, following Chapman et al. (2000), using the early grain filling phenological stage as the reference point. In this context, negative thermal time values represent phenological states prior to early grain filling, while positive values represent phenological stages after early grain filling. Before clustering, the data was organized by arranging the simulations as rows and the WS factors for each thermal time group as columns. The optimal number of clusters was determined using the *NbClust* (Charrad et al., 2014) package in the statistical programming language R (R Core Team, 2024), which employs 30 indexes to define the best number of clusters, selecting the most frequently recommended value.

A geospatial clustering approach was employed to identify spatially homogeneous regions with similar yield responses to different managements practices (planting date and MG). Mean yield and its coefficient of variation were computed to quantify central tendency and dispersion, respectively, for each combination of location, planting date, and genotype. A

neighborhood structure was established using a threshold distance of 150 kilometers, implemented through the *spdep* package (Bivand et al., 2013). Weights for this spatial structure were assigned using the inverse distance method. The *NbClust* package (Charrad et al., 2014) was employed to determine the optimal number of clusters. The clustering was implemented using the Spatial Fuzzy c-means (SFCM) algorithm from the *geocmeans* package (Jeremy, 2023), capitalizing on both the yield-related and spatial information. The SFCM algorithm was configured with four clusters (k = 4), a fuzziness coefficient of 3 (m = 3), and a spatial penalty parameter of 2 (alpha = 2). The fuzziness coefficient determines the softness of the cluster boundaries by allowing points to belong to multiple clusters to varying degrees, while the spatial penalty parameter integrates spatial proximity into the clustering process, promoting the formation of geographically coherent clusters. The chosen parameters balance cluster flexibility and spatial coherence, enabling meaningful overlap and geographic continuity in the data. The algorithm performed internal data standardization internally and utilized a median-based lag method to incorporate spatial dependency.

The crop seasons were classified into El Niño Southern Oscillation phases, based on the National Oceanic and Atmospheric Administration (NOAA). This classification employs the Pacific Ocean Sea surface temperature anomaly (SSTA) in relation to the normal in the El Niño 3.4 region. A given growing season was classified as El Niño when the mean SSTA is equal to or above 0.5 °C for the period between October and April. When the SSTA was equal to or below -0.5 °C for the period between October and April it was considered La Niña. A Neutral year was characterized when the SSTA remained between -0.5 and 0.5 °C.

The failure risk was determined as the percentage of simulations yielding less than the economic break-even yield for soybeans yield in a given scenario. The economic break-even

yield was calculated by the ratio between the cost of production and the grain price over the past five seasons (2019/2020 – 2023/2024) (CONAB, 2024). The overall failure risk was assessed by ENSO phase for each region, and further based on MG and planting date. For the soybean seed yield assessment, the average seed yield of each region was calculated and used as the reference to further assess the yield difference within each region.

A linear mixed-effects model was applied to assess the management impact on yield. The interactions among planting date, genotype, and ENSO and their main effects were treated as fixed effects, while the season with the location nested within the season was treated as the random effect. The crop yield was the response variable. This model was fitted using the *lme4* R package (Bates et al., 2015). To ensure the validity of our model, the standardized residuals were compared against the fitted values to check for the assumptions of normality and equal variance (Zuur et al., 2009). An ANOVA test with type III sum of squares was employed to test treatment effects, through the *car* package (Fox and Weisberg, 2018). All steps of the statistical analysis were carried out using the R software (R Core Team, 2024).

A summary of the methods is detailed in the framework shown in **Figure 2.1.**

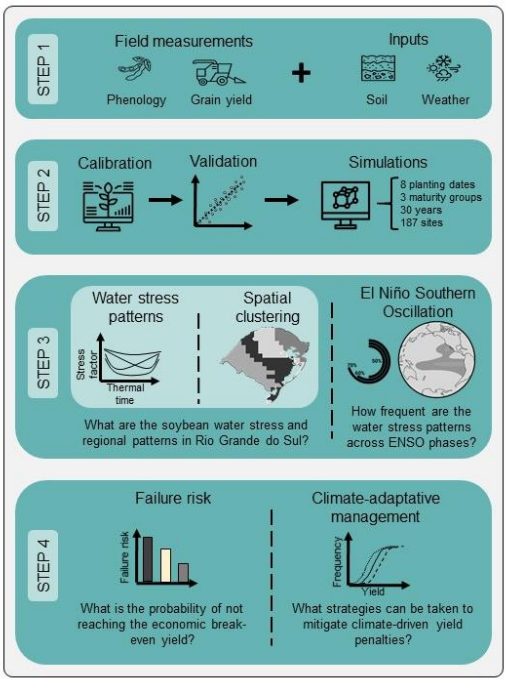


Figure 2.1. Workflow diagram highlighting the data collection before crop modeling investigation (Step 1), crop modeling structure (Step 2), characterization of water stress patterns and regions linked to ENSO phases (Step 3), and assessment of failure risk and development of climate-adaptative management strategies to counteract climate-driven yield penalties (Step 4).

Results

Model validation

The model parametrization achieved adequate crop phenology approximation, with an average RRMSE of 15 and 9%, ranging from 9 to 22 and 5 and 12, for days to flowering and days to maturity, respectively, across MGs and weather type. Likewise, the average yield RRMSE was 24%, varying from 16 (MG 6.4 – Cold and wet) to 35% (MG 5.0 – Hot and dry). For all MGs, hot and dry, and cold and wetseasons resulted in the highest and lowest yield RRMSE (31% and 19% on average), respectively (**Table 2.1, Figure 2.2B, 2.2C, 2.2D**). The median in-season precipitation and temperature across all validation environments was 689 mm and 23.2^{o}C, respectively (**Figure 2.2A**).

Table 2.1. Model validation metrics across maturity groups and weather types. Root mean square error (RMSE) and relative root mean square error for days to flowering, days to maturity and yield.

Maturity group	Weather type	RMSE			RRMSE		
-	-	Flowering	Maturity	Yield	Flowering	Maturity	Yield
		Days	Days	Mg ha^{-1}		%	
MG 5.0	Cold and dry	7.7	5.0	1.2	21	5	29
MG 5.0	Cold and wet	7.8	10	0.9	21	9	23
MG 5.0	Hot and dry	6.2	5.4	1.4	20	5	35
MG 5.0	Hot and wet	7.4	10	1.0	22	9	23
MG 5.8	Cold and dry	6.7	15	0.8	13	12	21
MG 5.8	Cold and wet	6.2	15	0.9	12	12	19
MG 5.8	Hot and dry	5.4	9.5	1.2	12	8	31
MG 5.8	Hot and wet	5.3	11	1.1	12	9	21
MG 6.4	Cold and dry	8.5	15	0.8	15	12	21
MG 6.4	Cold and wet	6.2	11	0.7	11	9	16
MG 6.4	Hot and dry	4.7	10	1.1	9	8	28
MG 6.4	Hot and wet	5.2	12	1.4	11	10	28

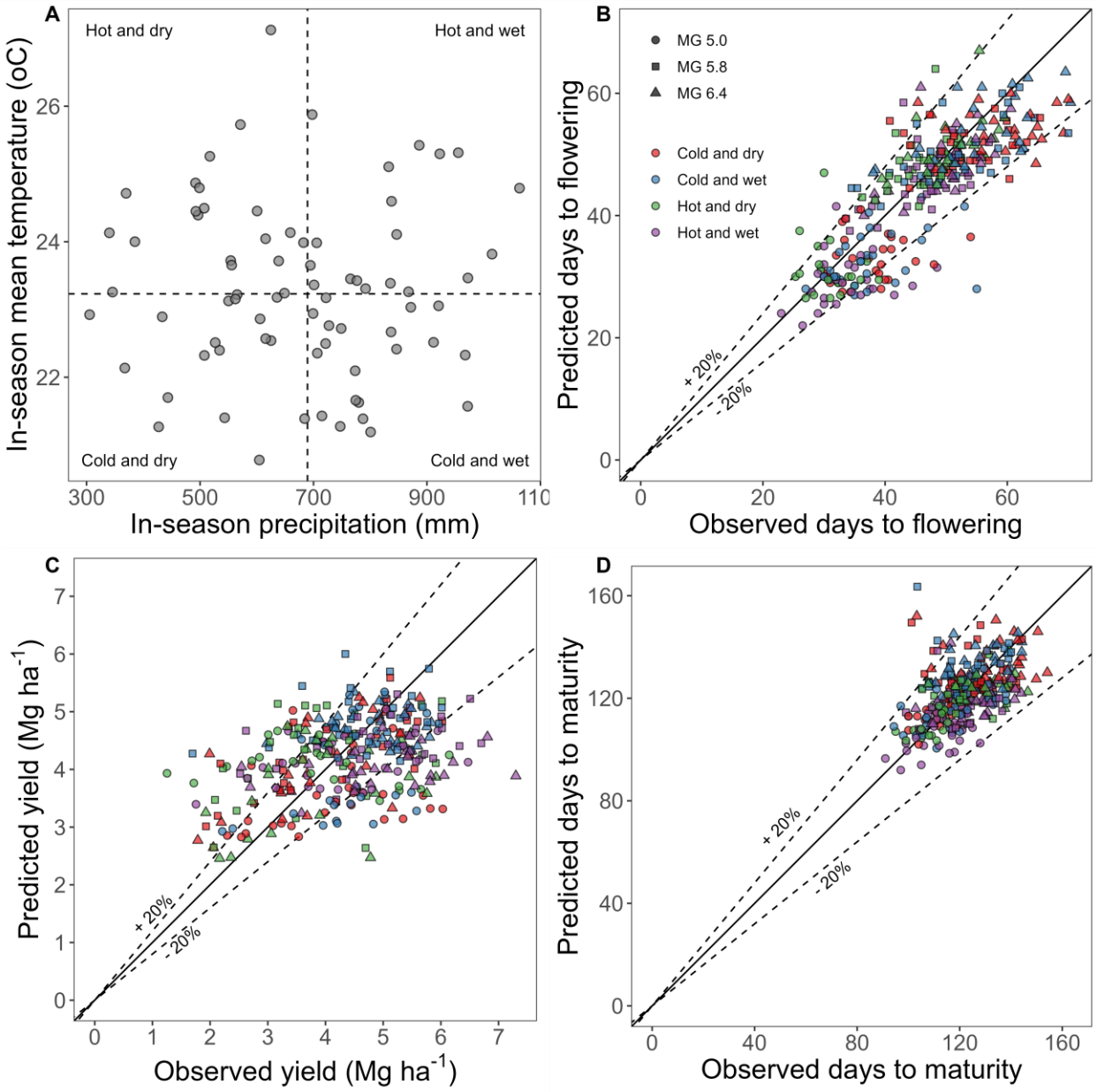


Figure 2.2. In-season weather characterization (A) and model validation (B, C, D). Vertical dashed lines in A correspond to the in-season median precipitation and mean temperature, respectively. In B, C and D, circles, squares, and triangles represent MGs 5.0, 5.8 and 6.4, respectively. Red, blue, green, and purple correspond to the weather types cold and dry, cold and wet, hot and dry, and hot and wet, respectively. In-silico results obtained using APSIM crop growth model.

Spatial clustering, water stress, environmental type classification, and soybean yield dynamics

Four distinct WS patterns were identified: no stress (WS factor over 0.75), early stress (WS factor ~0.5 at 500 ^{o}C days^{-1} before flowering), late stress (WS factor ~0.5 at flowering), and whole-season stress (WS factor under 0.5 from 400 ^{o}C days^{-1} before flowering to 200 ^{o}C days^{-1} after flowering) (**Figure 2.3A**). The whole season stress resulted in reductions on seed yield up to 50% (~2 Mg ha^{-1}) compared to no stress (~4 Mg ha^{-1}). Both early and late stress conditions resulted in intermediate average yields of ~3 Mg ha^{-1} (**Figure 2.3B**). Based on yield performance, four regions were classified: Northeast (NE), North (N), Central (C), and Southwest (SW) (**Figure 2.3B**). An average seed yield of 4.1, 3.4, 3.0, and 2.7 Mg ha^{-1} and a CV of 25, 26, 29, and 33 % were computed for the regions NE, N, C, and SW, respectively (**Figure 2.3C**). The most productive region (NE) presented the highest frequency of no stress pattern (~66%), while whole season stress was documented in only 5% of the simulations. On the other hand, the least productive region (SW) featured whole season stresses in one third of the simulations.

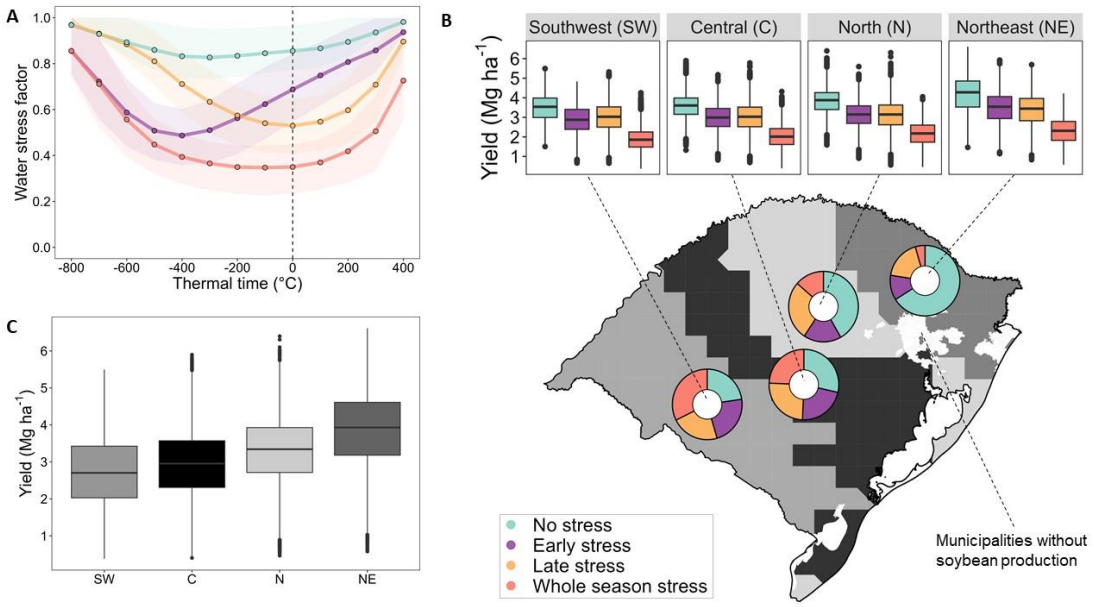


Figure 2.3. Soybean water stress patterns, clustered regions, and yield response: (A) water stress patterns. The relationship between water stress factor and crop development (thermal time). The vertical dashed line represents the early grain-filling phenological stage; (B) the distribution of soybean yield under varying water stress conditions in the four regions: Central (C), North (N), Northeast (NE), and Southwest (SW). The box plots illustrate the yield variability. The pie charts on the map, varying in color and size, represent the relative frequency of four categorized water stress patterns: no stress (green), early stress (purple), late stress (orange), and whole season stress (red) within each region; (C) distribution of soybean yields across the Southwest (SW), Central (C), North (N), and Northeast (NE) regions. In-silico results obtained using APSIM crop growth model.

Water stress and ENSO frequency

Over the past three decades, average seasonal ENSO phases have been distributed as follows: 41% La Niña, 31% Neutral, and 28% El Niño. Even though El Nino events were the less frequent, during its occurrence, the no stress pattern was predominant across regions, with frequencies of 90, 81, 56, and 45% in the NE, N, C, and SW regions, respectively. In contrast, La Nina events correlated with higher frequency of whole season stress in the C (35%) and SW (50%) regions. In Neutral events and under stress scenarios, the probability of late stress was superior to whole season and early stress. The NE region displayed a prevailing pattern of no stress across all ENSO phases (over 70%), with rare occurrences of whole-season stress (2%).

Within the N region, the majority of the Neutral seasons featured either no stress (40%) or late stress (37%) (**Figure 2.4)**.

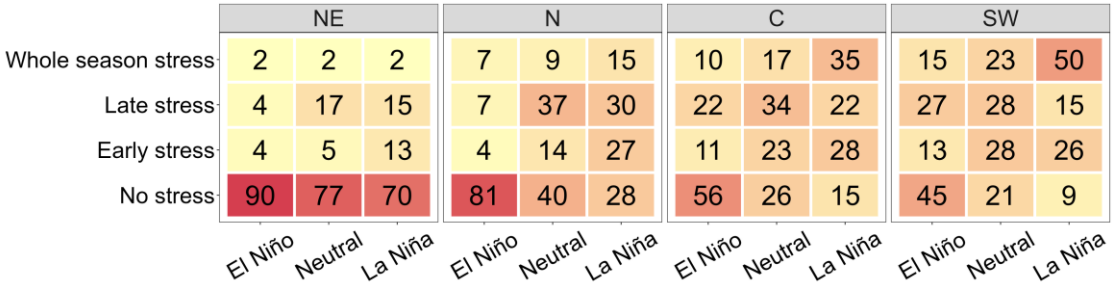


Figure 2.4. Frequency of water stress patterns across four regions during La Niña, Neutral, and El Niño phases. The heatmap conveys the percentage of stress occurrences, with color intensity indicating frequency. In-silico results obtained using APSIM crop growth model.

Climate-adaptative management strategies

Soybean seed yield was more variable in El Niño events than in Neutral and La Niña events in all regions studied (i.e., the cumulative frequency curves were wider) (**Figure 2.5**). The NE region showed the highest responsiveness to planting date and MG changes across all ENSO events, with a large gap of ~2.5 Mg ha^{-1} between the best (MG 5.8 at October 20th) and worst (MG 6.4 at January 20th) management combinations considering the 50% quantile. Early and intermediate planting dates (20-Oct and 5-Dec) correlated with higher yields during El Niño and Neutral events, while in La Niña events, this pattern was observed only in the NE region. In the other regions, there were no large differences in seed yield between planting dates. Although October 20th appeared as one of the most productive planting dates, for most of the scenarios there was a large gap between minimum and maximum seed yield (up to 5 Mg ha^{-1}), portraying high variability. On average, MG 5.8 outyielded MGs 5.0 and 6.4 by ~0.3 Mg ha^{-1} across all regions and ENSO phases (**Figure 2.5**).

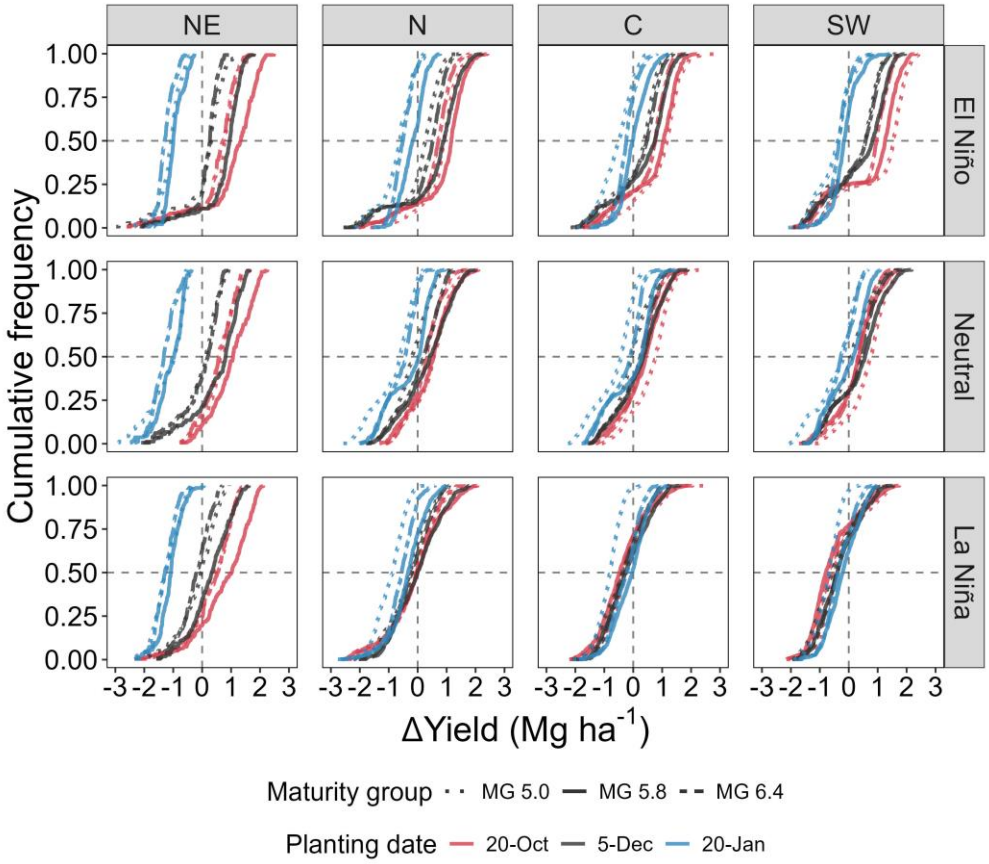


Figure 2.5. Cumulative frequency of yield across regions (columns), ENSO (rows), maturity groups (linetype), and planting dates (colors). Yield is expressed as the difference with the average of each region. In-silico results obtained using APSIM crop growth model.

Crop failure risk

The calculated mean economic break-even was 2.2 Mg ha^{-1}. A sensitivity analysis of failure risk using the 25, 50, and 75% quantiles of the economic break-even yield (1.5, 2.0, and 2.6 Mg ha^{-1}, respectively) can be found in **Appendix Figure A.3.** In the C region, the average failure risk probabilities during El Niño, Neutral, and La Niña were 13%, 16%, and 30%, while the N region had lower probabilities at 7%, 8%, and 12%. The SW region presented higher probabilities of 21, 20, and 48%. Conversely, the NE region maintained a consistently low failure chance of less than 3% for all ENSO phases. The ENSO led to a ~15 and 30% increase in crop failure risk in the regions C and SW during La Niña events, compared to Neutral and El

Niño seasons, which followed similar patterns of failure risk (**Figure 2.6A**). The shortest MG resulted in the greatest failure risks in all regions during La Nina events, reaching 40 to 50% of failure risk in the SW and C regions. In comparison, MGs 5.8 and 6.4 reported a reduced failure risk by approximately 10 to 15%. These two MGs showed similar failure risk across regions and ENSO phases (**Figure 2.6B**). Regarding planting dates, there was an increasing failure risk for the C and SW regions as planting was delayed during El Nino and Neutral events, peaking in late January, while in the NE region, it remained flat and under 10 % for all planting dates. La Nina events differed from Neutral and El Nino events mainly during early planting dates, resulting in higher failure risk compared to these events, reaching over 50% of risk in the SW region for October planting dates, for example (**Figure 2.6C**).

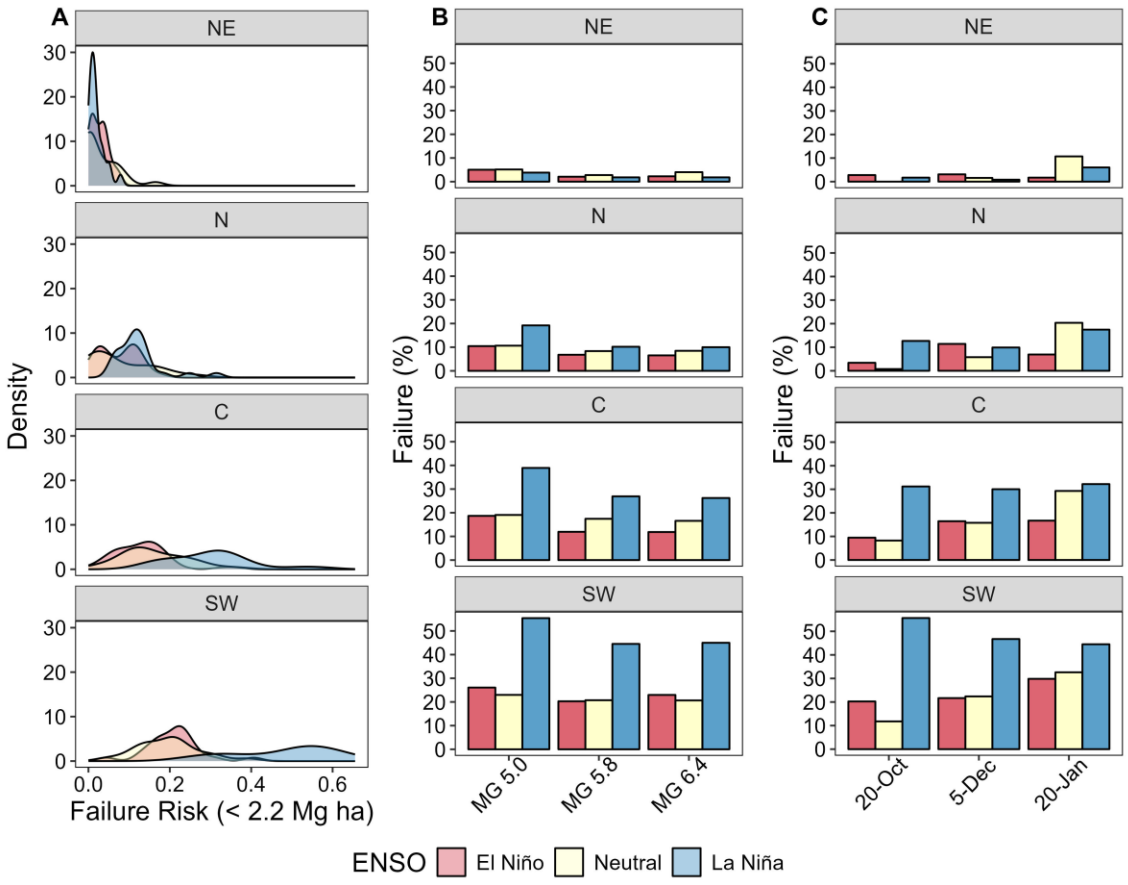


Figure 2.6. Comparative descriptive analysis of crop failure risk across different ENSO phases (colors): (A) Probability density functions for the four regions (panels) showing risk distribution under El Niño, Neutral, and La Niña conditions; (B) Percentage of crop failure associated with maturity groups (MGs) in each region; (C) Percentage of crop failure linked to planting dates. In-silico results obtained using APSIM crop growth model.

Discussion

This study offers valuable insights for developing targeted climate-adaptative management strategies to mitigate soybean failure risk and improve productivity in regions prone to WS in RS, Brazil. Previous efforts in the region supporting the use of ENSO phases to aid decision-making planting dates, ignored the impact of selecting the right soybean crop growth cycle on water management strategies (Nóia Júnior et al., 2020). Furthermore, there are still high uncertainties regarding the in-season weather at the time farmers need to make key management decisions (usually at sowing time), such as planting dates and MGs. Integrating advanced long-

term weather data and crop modeling tools can offer real-time insights and enhance the decision-making process. This study contributes to the global efforts of enhancing crop resilience through environmental WS characterization in the face of climate uncertainties in several crops (Chapman et al., 2000; Chenu et al., 2011), including soybeans (Battisti and Sentelhas, 2019).

Expanding upon this, up to 60% of yield variability in key agricultural regions is influenced by climate variation, with global climate variability accounting for approximately a third yield fluctuations (Ray et al., 2015). Particularly for Southern Brazil, water deficits have been identified as a major factor contributing to yield gaps, with an average loss 1.6 Mg ha^{-1} in soybean yields (Sentelhas et al., 2015). This study extends these findings by quantifying a potential yield penalty of up to 2 Mg ha^{-1}, specifically linked to the timing and severity of WS events. This WS induced yield penalty represents more than half of the average yield obtained during the best seasons in the RS state (CONAB, 2024). By pinpointing the impact of WS timing, this research enhances the understanding of climate-induced yield variability, contributing to a more resilient agricultural system globally. Furthermore, environmental characterizations describing the main production limitations are crucial for breeding programs and future environtyping efforts (Cooper et al., 2022; Resende et al., 2021). The results from our study suggest that there is a regional climatic variability within RS, with the SW region being more susceptible to prolonged stress events, and the NE region being less prone to WS. This marked sensitivity to La Nina phases towards the south of RS was also underscored by Nóia Júnior et al. (2020). Additionally, the southmost regions (C and SW) were more affected by La Nina years, with more frequent occurrence of stresses. The lower total precipitation and higher average temperature combined with lower soil water holding capacity, also reflected in the WS

frequency, pose as the main causing factors of this regional yield gap (Avila et al., 1996; Cunha et al., 2001).

Effective risk management is integral to agricultural decision-making, yet the adoption of quantitative predictive tools remains low due to knowledge-transfer barriers (Rose et al., 2016), and insufficient consideration of risk exposure and inherent uncertainties within production systems (Marra et al., 2003). In this regard, the interactions among planting dates, genotype maturity, and different ENSO phases offer a strategic avenue for minimizing failure risk and mitigating yield penalties (Boer and Surmaini, 2020; Hammer et al., 2014; Ramirez-Rodrigues et al., 2014). Optimum MGs and planting dates vary with weather scenarios (Di Mauro et al., 2022; Nóia Júnior et al., 2020; Nóia Júnior and Sentelhas, 2019; Videla-Mensegue et al., 2024), supporting the need for climate-adaptive management strategies. Similarly to this study, Di Mauro et al. (2022) reported that longer MGs were beneficial in La Nina phases for a similar region. Furthermore, in this study, early and intermediate planting dates (October 20th and December 5th) demonstrated promising performance attributed to increased radiation (Bhatia et al., 2008; Kumagai and Takahashi, 2020; Zanon et al., 2016) in alignment with the results from Nóia Júnior et al. (2020). However, in those environments, high variability and greater failure risk during La Nina phases underscored the importance of synchronizing critical growth stages combined with optimal weather conditions to avoid deficits during these stages (Eck et al., 1987; Nóia Júnior and Sentelhas, 2019; Zanon et al., 2016). Particularly in the southmost regions (SW and C), the election of longer MG played a critical role to reduce the failure risk (reduction of ~15%) during La Nina events. The later scenario clearly highlights the influence of the variation in both rainfall and temperature on soybean yields (Ferreira and Rao, 2011).

Similarly to previous studies using crop growth models, the predicted yield presented a typical tail pattern, overestimating the crop yield in low-yielding environments and underestimating it in high-yielding environments (Battisti and Sentelhas, 2019; van Versendaal et al., 2023). Additionally, challenges in predicting hot and dry seasons suggest that there is a need for improvements in the ability of the crop model assess plant water availability and temperature stresses. Likewise, Battisti et al. (2017) reported that the overestimation of yield under extreme water deficit is a limitation of model that needs to be addressed mainly focusing on crop water uptake and root growth capacity. Potential limitations of this study include the absence of calibration of crop genetic parameters that regulate plant biomass and leaf area index, as this study focused on yield and not intermediate products. In addition, there is a large variability in the performance of specific genotypes within a given MG due to characteristics such as root disease susceptibility and drought and heat tolerance that are not considered in most mechanistic models. Future research should focus on the genetic basis of stress tolerance (Dubey et al., 2019) and developing predictive platforms to refine climate-driven management strategies accounting for the seasonal variability of the SSTA. The nuanced understanding of WS impacts and heat stresses, as highlighted by Cohen et al. (2021), further emphasizes the need for targeted breeding x environmental x management practices. By leveraging advanced approaches, agricultural stakeholders can better anticipate and adapt to climatic risks, ultimately improving the resiliency of their agricultural farming systems under future climate shocks.

Conclusions

Soybean yield presented a penalty up to 2 Mg ha^{-1} under severe WS conditions, emphasizing the need to understand regional stress patterns to inform management strategies. The SW region was more susceptible to prolonged stress events, while the NE region was less

prone to experiencing WS. Climate-adaptative management strategies, such as optimizing planting dates and MGs, resulted in a 15% reduction in crop failure. Overall, these findings provide valuable insights for developing targeted approaches to enhance soybean yield stability, increasing farming resilience in the face of future climate uncertainties.

Acknowledgements

Contribution no. 25-123-J for the Kansas Research Experiment Station.

References

Alvares, C.A., Stape, J.L., Sentelhas, P.C., De Moraes Gonçalves, J.L., Sparovek, G., 2013. Köppen's climate classification map for Brazil. metz 22, 711–728. https://doi.org/10.1127/0941-2948/2013/0507

ANA lança mapeamento com dados atualizados sobre agricultura irrigada por pivôs centrais no Brasil [WWW Document], n.d. . Agência Nacional de Águas e Saneamento Básico (ANA). URL https://www.gov.br/ana/pt-br/ana-lanca-mapeamento-com-dados-atualizados-sobre-agricultura-irrigada-por-pivos-centrais-no-brasil (accessed 4.29.24).

Avila, A.M.H., Berlato, M.A., Silva, J.B., Fontana, D.C., 1996. PROBABILIDADE DE OCORRÊNCIA DE PRECIPITAÇÃO PLUVIAL MENSAL IGUAL OU MAIOR QUE A EVAPOTRANSPIRAÇÃO POTENCIAL PARA A ESTAÇÃO DE CRESCIMENTO DAS CULTURAS DE PRIMAVERA-VERÃO NO ESTADO DO RIO GRANDE DO SUL. Pesquisa Agropecuária Gaúcha 2, 149–154.

Basche, A.D., Archontoulis, S.V., Kaspar, T.C., Jaynes, D.B., Parkin, T.B., Miguez, F.E., 2016. Simulating long-term impacts of cover crops and climate change on crop production and environmental outcomes in the Midwestern United States. Agriculture, Ecosystems & Environment 218, 95–106. https://doi.org/10.1016/j.agee.2015.11.011

Bates, D., Mächler, M., Bolker, B., Walker, S., 2015. Fitting Linear Mixed-Effects Models Using lme4. Journal of Statistical Software 67, 1–48. https://doi.org/10.18637/jss.v067.i01

Battisti, R., Casaroli, D., Paixão, J.S., Alves Júnior, J., Evangelista, A.W.P., Mesquita, M., 2020a. Assessment of Soybeans Crop Management Strategies Using Crop Growth Models for Central Brazil, in: Mirschel, W., Terleev, V.V., Wenkel, K.-O. (Eds.), Landscape Modelling and Decision Support, Innovations in Landscape Research. Springer International Publishing, Cham, pp. 525–543. https://doi.org/10.1007/978-3-030-37421-1_27

Battisti, R., Ferreira, M.D.P., Tavares, É.B., Knapp, F.M., Bender, F.D., Casaroli, D., Alves Júnior, J., 2020b. Rules for grown soybean-maize cropping system in Midwestern Brazil: Food

production and economic profits. Agricultural Systems 182, 102850. https://doi.org/10.1016/j.agsy.2020.102850

Battisti, R., Sentelhas, P.C., 2019. Characterizing Brazilian soybean-growing regions by water deficit patterns. Field Crops Research 240, 95–105. https://doi.org/10.1016/j.fcr.2019.06.007

Battisti, R., Sentelhas, P.C., Boote, K.J., 2017. Inter-comparison of performance of soybean crop simulation models and their ensemble in southern Brazil. Field Crops Research 200, 28–37. https://doi.org/10.1016/j.fcr.2016.10.004

Battisti, R., Sentelhas, P.C., Parker, P.S., Nendel, C., Câmara, G.M.D.S., Farias, J.R.B., Basso, C.J., 2018. Assessment of crop-management strategies to improve soybean resilience to climate change in Southern Brazil. Crop Pasture Sci. 69, 154–162. https://doi.org/10.1071/CP17293

Bhatia, V.S., Singh, P., Wani, S.P., Chauhan, G.S., Rao, A.V.R.K., Mishra, A.K., Srinivas, K., 2008. Analysis of potential yields and yield gaps of rainfed soybean in India using CROPGRO-Soybean model. Agricultural and Forest Meteorology 148, 1252–1265. https://doi.org/10.1016/j.agrformet.2008.03.004

Bivand, R.S., Pebesma, E., Gómez-Rubio, V., 2013. Applied Spatial Data Analysis with R. Springer, New York, NY. https://doi.org/10.1007/978-1-4614-7618-4

Boer, R., Surmaini, E., 2020. Economic benefits of ENSO information in crop management decisions: case study of rice farming in West Java, Indonesia. Theor Appl Climatol 139, 1435–1446. https://doi.org/10.1007/s00704-019-03055-9

Boote, K.J., Jones, J.W., Pickering, N.B., 1996. Potential Uses and Limitations of Crop Models. Agronomy Journal 88, 704–716. https://doi.org/10.2134/agronj1996.00021962008800050005x

Brauman, K.A., Siebert, S., Foley, J.A., 2013. Improvements in crop water productivity increase water sustainability and food security—a global analysis. Environ. Res. Lett. 8, 024030. https://doi.org/10.1088/1748-9326/8/2/024030

Brown, H.E., Huth, N.I., Holzworth, D.P., Teixeira, E.I., Zyskowski, R.F., Hargreaves, J.N.G., Moot, D.J., 2014. Plant Modelling Framework: Software for building and running crop models on the APSIM platform. Environmental Modelling & Software 62, 385–398. https://doi.org/10.1016/j.envsoft.2014.09.005

Cai, W., McPhaden, M.J., Grimm, A.M., Rodrigues, R.R., Taschetto, A.S., Garreaud, R.D., Dewitte, B., Poveda, G., Ham, Y.-G., Santoso, A., Ng, B., Anderson, W., Wang, G., Geng, T., Jo, H.-S., Marengo, J.A., Alves, L.M., Osman, M., Li, S., Wu, L., Karamperidou, C., Takahashi, K., Vera, C., 2020. Climate impacts of the El Niño–Southern Oscillation on South America. Nat Rev Earth Environ 1, 215–231. https://doi.org/10.1038/s43017-020-0040-3

Chapman, S.C., Cooper, M., Hammer, G.L., Butler, D.G., 2000. Genotype by environment interactions affecting grain sorghum. II. Frequencies of different seasonal patterns of drought stress are related to location effects on hybrid yields. Aust. J. Agric. Res. 51, 209–222. https://doi.org/10.1071/ar99021

Charrad, M., Ghazzali, N., Boiteau, V., Niknafs, A., 2014. NbClust: An R Package for Determining the Relevant Number of Clusters in a Data Set. Journal of Statistical Software 61, 1–36. https://doi.org/10.18637/jss.v061.i06

Chenu, K., Cooper, M., Hammer, G.L., Mathews, K.L., Dreccer, M.F., Chapman, S.C., 2011. Environment characterization as an aid to wheat improvement: interpreting genotype–environment interactions by modelling water-deficit patterns in North-Eastern Australia. Journal of Experimental Botany 62, 1743–1755. https://doi.org/10.1093/jxb/erq459

Cohen, I., Zandalinas, S.I., Fritschi, F.B., Sengupta, S., Fichman, Y., Azad, R.K., Mittler, R., 2021. The impact of water deficit and heat stress combination on the molecular response, physiology, and seed production of soybean. Physiologia Plantarum 172, 41–52. https://doi.org/10.1111/ppl.13269

Conab - Página inicial [WWW Document], n.d. URL https://www.conab.gov.br/ (accessed 6.10.24).

Cooper, M., Messina, C.D., Tang, T., Gho, C., Powell, O.M., Podlich, D.W., Technow, F., Hammer, G.L., 2022. Predicting Genotype × Environment × Management (G × E × M) Interactions for the Design of Crop Improvement Strategies, in: Plant Breeding Reviews. John Wiley & Sons, Ltd, pp. 467–585. https://doi.org/10.1002/9781119874157.ch8

Cunha, G., Barni, N.A., Haas, J.C., Maluf, J.R.T., Matzenauer, R., Pasinato, A., Pimentel, M.B.M., Pires, J., 2001. Zoneamento agrícola e época de semeadura para soja no Rio Grande do Sul. Revista Brasileira de Agrometeorologia 9, 446–459.

Di Mauro, G., Parra, G., Santos, D.J., Enrico, J.M., Zuil, S., Murgio, M., Zbinden, F., Costanzi, J., Arias, N., Carrio, A., Vissani, C., Fuentes, F., Salvagiotti, F., 2022. Defining soybean maturity group options for contrasting weather scenarios in the American Southern Cone. Field Crops Research 287, 108676. https://doi.org/10.1016/j.fcr.2022.108676

Du, Y., Zhao, Q., Chen, L., Yao, X., Zhang, H., Wu, J., Xie, F., 2020. Effect of Drought Stress during Soybean R2–R6 Growth Stages on Sucrose Metabolism in Leaf and Seed. International Journal of Molecular Sciences 21, 618. https://doi.org/10.3390/ijms21020618

Duan, Z., Li, Q., Wang, H., He, X., Zhang, M., 2023. Genetic regulatory networks of soybean seed size, oil and protein contents. Frontiers in Plant Science 14.

Dubey, A., Kumar, A., Abd_Allah, E.F., Hashem, A., Khan, M.L., 2019. Growing more with less: Breeding and developing drought resilient soybean to improve food security. Ecological Indicators 105, 425–437. https://doi.org/10.1016/j.ecolind.2018.03.003

Eck, H.V., Mathers, A.C., Musick, J.T., 1987. Plant water stress at various growth stages and growth and yield of soybeans. Field Crops Research 17, 1–16. https://doi.org/10.1016/0378-4290(87)90077-3

Ferreira, D.B., Rao, V.B., 2011. Recent climate variability and its impacts on soybean yields in Southern Brazil. Theor Appl Climatol 105, 83–97. https://doi.org/10.1007/s00704-010-0358-8

Figueiredo Moura da Silva, E.H., Silva Antolin, L.A., Zanon, A.J., Soares Andrade, A., Antunes de Souza, H., dos Santos Carvalho, K., Aparecido Vieira, N., Marin, F.R., 2021. Impact assessment of soybean yield and water productivity in Brazil due to climate change. European Journal of Agronomy 129, 126329. https://doi.org/10.1016/j.eja.2021.126329

Fox, J., Weisberg, S., 2018. An R Companion to Applied Regression. SAGE Publications.

Fuentes-Llanillo, R., Telles, T.S., Soares Junior, D., de Melo, T.R., Friedrich, T., Kassam, A., 2021. Expansion of no-tillage practice in conservation agriculture in Brazil. Soil and Tillage Research 208, 104877. https://doi.org/10.1016/j.still.2020.104877

Funk, C., Peterson, P., Landsfeld, M., Pedreros, D., Verdin, J., Shukla, S., Husak, G., Rowland, J., Harrison, L., Hoell, A., Michaelsen, J., 2015. The climate hazards infrared precipitation with stations—a new environmental record for monitoring extremes. Sci Data 2, 150066. https://doi.org/10.1038/sdata.2015.66

Gebre, M.G., Earl, H.J., 2020. Effects of Growth Medium and Water Stress on Soybean [Glycine max (L.) Merr.] Growth, Soil Water Extraction and Rooting Profiles by Depth in 1-m Rooting Columns. Frontiers in Plant Science 11.

Hammer, G.L., McLean, G., Chapman, S., Zheng, B., Doherty, A., Harrison, M.T., Oosterom, E. van, Jordan, D., 2014. Crop design for specific adaptation in variable dryland production environments. Crop Pasture Sci. 65, 614–626. https://doi.org/10.1071/CP14088

Holzworth, D.P., Huth, N.I., deVoil, P.G., Zurcher, E.J., Herrmann, N.I., McLean, G., Chenu, K., van Oosterom, E.J., Snow, V., Murphy, C., Moore, A.D., Brown, H., Whish, J.P.M., Verrall, S., Fainges, J., Bell, L.W., Peake, A.S., Poulton, P.L., Hochman, Z., Thorburn, P.J., Gaydon, D.S., Dalgliesh, N.P., Rodriguez, D., Cox, H., Chapman, S., Doherty, A., Teixeira, E., Sharp, J., Cichota, R., Vogeler, I., Li, F.Y., Wang, E., Hammer, G.L., Robertson, M.J., Dimes, J.P., Whitbread, A.M., Hunt, J., van Rees, H., McClelland, T., Carberry, P.S., Hargreaves, J.N.G., MacLeod, N., McDonald, C., Harsdorf, J., Wedgwood, S., Keating, B.A., 2014. APSIM – Evolution towards a new generation of agricultural systems simulation. Environmental Modelling & Software 62, 327–350. https://doi.org/10.1016/j.envsoft.2014.07.009

Home | Food and Agriculture Organization of the United Nations [WWW Document], n.d. . FAOHome. URL https://www.fao.org/home/en (accessed 6.10.24).

IBGE | Portal do IBGE | IBGE [WWW Document], n.d. URL https://www.ibge.gov.br/ (accessed 3.18.24).

Iizumi, T., Luo, J.-J., Challinor, A.J., Sakurai, G., Yokozawa, M., Sakuma, H., Brown, M.E., Yamagata, T., 2014. Impacts of El Niño Southern Oscillation on the global yields of major crops. Nat Commun 5, 3712. https://doi.org/10.1038/ncomms4712

ISRIC — World Soil Information [WWW Document], n.d. . ISRIC — World Soil Information. URL https://www.isric.org (accessed 2.16.24).

Jeremy, G., 2023. geocmeans: An R package for spatial fuzzyc-means. JOSS 8, 5259. https://doi.org/10.21105/joss.05259

Keating, B.A., Carberry, P.S., Hammer, G.L., Probert, M.E., Robertson, M.J., Holzworth, D., Huth, N.I., Hargreaves, J.N.G., Meinke, H., Hochman, Z., McLean, G., Verburg, K., Snow, V., Dimes, J.P., Silburn, M., Wang, E., Brown, S., Bristow, K.L., Asseng, S., Chapman, S., McCown, R.L., Freebairn, D.M., Smith, C.J., 2003. An overview of APSIM, a model designed for farming systems simulation. European Journal of Agronomy, Modelling Cropping Systems: Science, Software and Applications 18, 267–288. https://doi.org/10.1016/S1161-0301(02)00108-9

Kukal, M.S., Irmak, S., 2018. Climate-Driven Crop Yield and Yield Variability and Climate Change Impacts on the U.S. Great Plains Agricultural Production. Sci Rep 8, 3450. https://doi.org/10.1038/s41598-018-21848-2

Kumagai, E., Takahashi, T., 2020. Soybean (Glycine max (L.) Merr.) Yield Reduction due to Late Sowing as a Function of Radiation Interception and Use in a Cool Region of Northern Japan. Agronomy 10, 66. https://doi.org/10.3390/agronomy10010066

Lobell, D.B., Schlenker, W., Costa-Roberts, J., 2011. Climate Trends and Global Crop Production Since 1980. Science 333, 616–620. https://doi.org/10.1126/science.1204531

Marra, M., Pannell, D.J., Abadi Ghadim, A., 2003. The economics of risk, uncertainty and learning in the adoption of new agricultural technologies: where are we on the learning curve? Agricultural Systems 75, 215–234. https://doi.org/10.1016/S0308-521X(02)00066-5

Martins, J.D., Petry, M.T., Motovanelli, B.C., Ferrazza, C.M., 2021. MAPEAMENTO DA ÁREA IRRIGADA POR PIVÔ CENTRAL EM NÍVEL DE BACIA HIDROGRÁFICA NO EXTREMO SUL DO BRASIL. IRRIGA 1, 281–296. https://doi.org/10.15809/irriga.2021v1n2p281-296

Miguez, F., 2024. apsimx: Inspect, Read, Edit and Run “APSIM” ‘Next Generation’ and “APSIM” Classic.

Mourtzinis, S., Specht, J.E., Lindsey, L.E., Wiebold, W.J., Ross, J., Nafziger, E.D., Kandel, H.J., Mueller, N., Devillez, P.L., Arriaga, F.J., Conley, S.P., 2015. Climate-induced reduction in US-wide soybean yields underpinned by region- and in-season-specific responses. Nature Plants 1, 1–4. https://doi.org/10.1038/nplants.2014.26

Nelder, J.A., Mead, R., 1965. A Simplex Method for Function Minimization. The Computer Journal 7, 308–313. https://doi.org/10.1093/comjnl/7.4.308

Nóia Júnior, R. de S., Fraisse, C.W., Karrei, M.A.Z., Cerbaro, V.A., Perondi, D., 2020. Effects of the El Niño Southern Oscillation phenomenon and sowing dates on soybean yield and on the occurrence of extreme weather events in southern Brazil. Agricultural and Forest Meteorology 290, 108038. https://doi.org/10.1016/j.agrformet.2020.108038

Nóia Júnior, R. de S., Sentelhas, P.C., 2019. Soybean-maize off-season double crop system in Brazil as affected by El Niño Southern Oscillation phases. Agricultural Systems 173, 254–267. https://doi.org/10.1016/j.agsy.2019.03.012

Perondi, D., de Souza Nóia Júnior, R., Zotarelli, L., Mulvaney, M.J., Fraisse, C.W., 2022. Soybean maturity groups and sowing dates to minimize ENSO and extreme weather events effects on yield variability in the Southeastern US. Agricultural and Forest Meteorology 324, 109104. https://doi.org/10.1016/j.agrformet.2022.109104

Perondi, D., Fraisse, C.W., Watson, J.A., Boote, K.J., Zotarelli, L., Huffaker, R.G., 2023. Assessing the impact of sowing dates and ENSO in a drought index-based insurance for soybean. Climate Risk Management 41, 100544. https://doi.org/10.1016/j.crm.2023.100544

Peterson, C.A., Bell, L.W., Carvalho, P.C. de F., Gaudin, A.C.M., 2020. Resilience of an Integrated Crop–Livestock System to Climate Change: A Simulation Analysis of Cover Crop Grazing in Southern Brazil. Frontiers in Sustainable Food Systems 4.

Pierre Pott, L., Jorge Carneiro Amado, T., Augusto Schwalbert, R., Mateus Corassa, G., Antonio Ciampitti, I., 2022. Crop type classification in Southern Brazil: Integrating remote sensing, crop modeling and machine learning. Computers and Electronics in Agriculture 201, 107320. https://doi.org/10.1016/j.compag.2022.107320

Poggio, L., de Sousa, L.M., Batjes, N.H., Heuvelink, G.B.M., Kempen, B., Ribeiro, E., Rossiter, D., 2021. SoilGrids 2.0: producing soil information for the globe with quantified spatial uncertainty. SOIL 7, 217–240. https://doi.org/10.5194/soil-7-217-2021

Probert, M.E., Delve, R.J., Kimani, S.K., Dimes, J.P., n.d. The APSIM Manure Module: Improvements in Predictability and Application to Laboratory Studies.

Probert, M.E., Dimes, J.P., Keating, B.A., Dalal, R.C., Strong, W.M., 1998. APSIM's water and nitrogen modules and simulation of the dynamics of water and nitrogen in fallow systems. Agricultural Systems 56, 1–28. https://doi.org/10.1016/S0308-521X(97)00028-0

R: The R Project for Statistical Computing [WWW Document], n.d. URL https://www.r-project.org/ (accessed 2.14.24).

Ramirez-Rodrigues, M.A., Asseng, S., Fraisse, C., Stefanova, L., Eisenkolbi, A., 2014. Tailoring wheat management to ENSO phases for increased wheat production in Paraguay. Climate Risk Management 3, 24–38. https://doi.org/10.1016/j.crm.2014.06.001

Ray, D.K., Gerber, J.S., MacDonald, G.K., West, P.C., 2015. Climate variation explains a third of global crop yield variability. Nat Commun 6, 5989. https://doi.org/10.1038/ncomms6989

Resende, R.T., Piepho, H.-P., Rosa, G.J.M., Silva-Junior, O.B., e Silva, F.F., de Resende, M.D.V., Grattapaglia, D., 2021. Enviromics in breeding: applications and perspectives on envirotypic-assisted selection. Theor Appl Genet 134, 95–112. https://doi.org/10.1007/s00122-020-03684-z

Rezaei, E.E., Webber, H., Asseng, S., Boote, K., Durand, J.L., Ewert, F., Martre, P., MacCarthy, D.S., 2023. Climate change impacts on crop yields. Nat Rev Earth Environ 4, 831–846. https://doi.org/10.1038/s43017-023-00491-0

Robertson, M.J., Carberry, P.S., Huth, N.I., Turpin, J.E., Probert, M.E., Poulton, P.L., Bell, M., Wright, G.C., Yeates, S.J., Brinsmead, R.B., 2002. Simulation of growth and development of diverse legume species in APSIM. Aust. J. Agric. Res. 53, 429–446. https://doi.org/10.1071/ar01106

Ropelewski, C.F., Halpert, M.S., 1987. Global and Regional Scale Precipitation Patterns Associated with the El Niño/Southern Oscillation. Monthly Weather Review 115, 1606–1626. https://doi.org/10.1175/1520-0493(1987)115<1606:GARSPP>2.0.CO;2

Rose, D.C., Sutherland, W.J., Parker, C., Lobley, M., Winter, M., Morris, C., Twining, S., Ffoulkes, C., Amano, T., Dicks, L.V., 2016. Decision support tools for agriculture: Towards effective design and delivery. Agricultural Systems 149, 165–174. https://doi.org/10.1016/j.agsy.2016.09.009

Santos, H.G. dos, Jacomine, P.K.T., Anjos, L.H.C. dos, Oliveira, V.A. de, Lumbreras, J.F., Coelho, M.R., Almeida, J.A. de, Araujo Filho, J.C. de, Oliveira, J.B. de, Cunha, T.J.F., 2018. Sistema Brasileiro de Classificação de Solos. Brasília, DF: Embrapa, 2018.

Sentelhas, P.C., Battisti, R., Câmara, G.M.S., Farias, J.R.B., Hampf, A.C., Nendel, C., 2015. The soybean yield gap in Brazil - Magnitude, causes and possible solutions for sustainable production. Journal of Agricultural Science 153, 1394–1411. https://doi.org/10.1017/S0021859615000313

Tecnologia, I., n.d. Center for Advanced Studies on Applied Economics [WWW Document]. Center for Advanced Studies on Applied Economics. URL https://cepea.esalq.usp.br/en (accessed 6.10.24).

Thorburn, P.J., Probert, M.E., Robertson, F.A., 2001. Modelling decomposition of sugar cane surface residues with APSIM–Residue. Field Crops Research 70, 223–232. https://doi.org/10.1016/S0378-4290(01)00141-1

Turek, M.E., Poggio, L., Batjes, N.H., Armindo, R.A., de Jong van Lier, Q., de Sousa, L., Heuvelink, G.B.M., 2023. Global mapping of volumetric water retention at 100, 330 and 15 000 cm suction using the WoSIS database. International Soil and Water Conservation Research 11, 225–239. https://doi.org/10.1016/j.iswcr.2022.08.001

van Versendaal, E., Carcedo, A.J.P., Adee, E., Sassenrath, G., Dooley, S., Lingenfelser, J., Ciampitti, I.A., 2023. Integrating Field Data and a Modeling Approach to Inform Optimum Planting Date × Maturity Group for Soybeans under Current and Future Weather Conditions in Kansas. Sustainability 15, 1081. https://doi.org/10.3390/su15021081

Videla-Mensegue, H., Caviglia, O.P., Degioanni, A., Marcos, J., Bonadeo, E., 2021. Modelling water productivity for ecological intensification of crop sequences in the Inner Argentinean Pampas. Field Crops Research 271, 108246. https://doi.org/10.1016/j.fcr.2021.108246

Videla-Mensegue, H., Córdoba, M., Caviglia, O.P., Sadras, V.O., 2024. Soybean yield and water productivity gaps associate with ENSO-dependent effects of fungicide, sowing date and maturity group. European Journal of Agronomy 155, 127133. https://doi.org/10.1016/j.eja.2024.127133

Wallach, D., Makowski, D., Jones, J.W., Brun, F., 2018. Working with Dynamic Crop Models: Methods, Tools and Examples for Agriculture and Environment. Academic Press.

Wang, S., Liu, S., Wang, J., Yokosho, K., Zhou, B., Yu, Y.-C., Liu, Z., Frommer, W.B., Ma, J.F., Chen, L.-Q., Guan, Y., Shou, H., Tian, Z., 2020. Simultaneous changes in seed size, oil content and protein content driven by selection of SWEET homologues during soybean domestication. National Science Review 7, 1776–1786. https://doi.org/10.1093/nsr/nwaa110

Zanon, A.J., Streck, N.A., Grassini, P., 2016. Climate and Management Factors Influence Soybean Yield Potential in a Subtropical Environment. Agronomy Journal 108, 1447–1454. https://doi.org/10.2134/agronj2015.0535

Zuur, A.F., Ieno, E.N., Walker, N., Saveliev, A.A., Smith, G.M., 2009. Mixed effects models and extensions in ecology with R, Statistics for Biology and Health. Springer, New York, NY. https://doi.org/10.1007/978-0-387-87458-6

Chapter 3 - Soybean Critical N Dilution Curve Using Non-nodulating Genotypes

Under review in Plant and Soil Journal.

Abstract

The critical nitrogen (N) dilution curve defines the minimum plant N concentration (%Nc) required to maximize crop growth, which is essential for diagnosing plant N status. Soybeans (*Glycine max* L.) pose a challenge due to the contribution of biological N fixation in addition to soil N. This study aims to: i) review the current scientific knowledge on N dilution curves for soybeans; ii) establish a critical N dilution curve using non-nodulating genotypes; and iii) study the main physiological mechanisms underpinning soybean N demand. A literature review was conducted to compile data on soybean N dilution curves. A field experiment was conducted using four soybean genotypes (two nodulating and two non-nodulating) under four fertilizer N rates (0, 100, 200, and 300 kg N ha^{-1}). Non-nodulating soybeans exhibited a 46% greater N dilution than their nodulating counterparts. Nodulating genotypes reported greater specific leaf area (20%) and specific leaf nitrogen (45%), with a reduction in the specific leaf weight (17%). The intrinsic N capacity increased not only for the leaf organ but in a similar proportion in stem and pod tissues, all acting as N reservoirs for satisfying seed N demand. Soil-%Nc followed typical dilution with increasing biomass, while atmospheric-%Nc increased during growth.A critical N dilution curve in soybeans was established using non-nodulating genotypes, revealing greater dilution than previously reported in the literature for nodulating soybeans. It also highlighted the importance of N reservoir in enhancing light interception and increasing plant N content in nodulating soybeans.

Introduction

The nitrogen (N) dilution curve has been used as a diagnostic tool for N status in wheat (*Triticum aestivum* L.) (Justes et al., 1994), maize (*Zea mays* L.) (Plénet and Lemaire, 1999), and soybean (*Glycine max* L.) (Divito et al., 2016). The critical N dilution curve defines the minimum plant N concentration (%Nc) required to maximize crop growth, which decreases as the crop reaches maturity (Greenwood et al., 1990; Lemaire et al., 2008; Plénet and Lemaire, 1999). Several studies have reported N dilution curves for soybeans (Almeida et al., 2023; Divito et al., 2016; Ney et al., 1997; Salvagiotti et al., 2008; Santachiara et al., 2018), however, soybeans can access another N source (different from soil N) via the symbiosis with microorganisms that fix atmospheric N via the N fixation process. Therefore, the critical N dilution curve for soybeans has not yet been determined due to the complexity of considering the plant N dilution including both N sources, soil plus N fixation processes. To determine the critical N dilution for soybeans both N sources should be segregated, thus, the introduction of non-nodulating isolines can aid in quantifying the critical plant N dilution when this crop is not relying on N fixation.

Crops generally respond to N deficiency by decreasing light interception, reducing canopy photosynthetic rate, or both. This trade-off involves balancing resource capture and optimizing use efficiency (Grindlay, 1997; Sinclair and Horie, 1989; Vos et al., 2005). In a N-limited environment, decreasing light interception and/or reducing photosynthesis rate are attempts to optimize the use of the available resources (Gastal et al., 2015). For example, in wheat, a reduction of the leaf area is expected to maintain specific leaf N (SLN) levels (Lemaire et al., 2008a). On the other hand, maize portrays a different approach with the priority of expanding the leaf area in detriment of a reduction in leaf N concentration, and plant N uptake

(Lemaire et al. 2008b; Gastal et al., 2015). Deficiencies in N also alters N allocation between the canopy and stem, with corn reducing N partitioning to the stem while wheat experiences minimal or no decrease (Gastal et al., 2015). These responses highlight differences in crop adaptation to N-limited environments, with corn being more sensitive to N deficiency in radiation use efficiency (RUE) than wheat, considering that ~60% of leaf N corresponds to proteins associated with photosynthetic apparatus (Evans, 1989). Although Lemaire et al. (2008) conceptualized these responses in several crops, there is limited information on how soybeans respond to N deficiency (due to the complexity of studying the N fixation process) and the main physiological mechanisms governing the response under variations in N status.

Following this rationale, this study aimed to: i) conduct a review to synthesize current knowledge on N dilution curves for soybeans, providing a benchmark for subsequent analysis; ii) define a critical N dilution curve using non-nodulating soybean genotypes; and iii) study the main physiological mechanisms governing the relationship between plant growth and N sources (soil and atmosphere) for this crop.

Methods

Review on soybean plant N dilution curve

Scientific publications reporting plant N dilution curves in soybeans were screened to extract their coefficients and the maximum plant biomass. These coefficients were used to parameterize the N dilution curve, for each unique publication utilizing a power model. For three of the curves the parameters were reported, so that the %Nc and plant biomass were extracted to calculate the parameters further described in 2.4.1.

Field experiment

Experimental design and growing conditions

The study has been conducted in Junction City, Kansas (39.074°N, -96.744°W), United States, during the 2023 growing season at an elevation of 321 m. The soil type is classified as Hapludoll with a silt-loam texture. The climate type is classified as Humid continental (Dfa) (Kottek et al., 2006). The crop was sown on May 17th and harvested on September 28th. Throughout the growing season, 255 mm of precipitation were accumulated, with an average maximum and minimum temperature of 31 and 17 °C, respectively (**Appendix Figure B.1**).

Treatments consisted of a factorial arrangement of four early maturity group 4 soybean genotypes (KS4120-1_rj1, KS4120-7-1_rj5/6, KS4120NSGT, and KS4120-7-2_Rj5/rj6, referred to as Non-nod1, Non-nod2, Nod1, and Nod2, respectively, and four fertilizer N rates (0, 100, 200 and 300 kg ha^{-1}) in a split-plot design with four replications. The fertilizer N rates were the main plots, and genotypes were assigned to the subplots. The non-nodulating near-isogenic line KS4120-1_rj1 was developed from the Harosoy-Nod non-nodulating source. The non-nodulating line KS4120-7-1_rj5/rj6 and nodulating line KS4120-7-2_Rj5/rj6 were derived from heterogeneous BC_4F_2 families from the William-NN source. The near-isogenic line, and the heterogeneous families were developed collaboratively by Kansas State University, the University of Arkansas, the U.S. Department of Agriculture and the University of Georgia. The recurrent parent, KS4120NSGT, was developed and released by the Kansas Agricultural Experiment Station. Non-nod1 and Non-nod2 genotypes possess nearly identical characteristics to Nod1 and Nod2, except that their nodulating genes were inhibited. The plot area was 54 m^2 (6 m wide by 9 m long) with a row spacing of 0.76 m. Nitrogen fertilizer was broadcasted as urea at crop emergence. The nodulating genotypes were inoculated with *Bradyrhizobium* sp. immediately prior to sowing by mixing the recommended number of seed thoroughly with the

required amount of inoculant (provided by Visjon Biologics, Henrietta, TX). Standard agronomic practices were adopted to manage pests, diseases, and weeds.

Field measurements and laboratory analyses

Prior to sowing, composite soil samples (6 cores) were taken from a 0-to-20 cm soil depth within each plot to characterize soil attributes such as pH, soil organic matter (OM), phosphorus (P), potassium (K), sulfur (S), calcium (Ca), magnesium (Mg), sodium (Na), nitrate (NO_3^-N), ammonium (NH_4^+-N), cation exchange capacity (CEC), and soil texture (sand, silt, and clay composition) (**Appendix Table B1**). Plant biomass was collected at the beginning of bloom (R1, 58 days after sowing [DAS]; full bloom, R2, 70 DAS; beginning pod development, R3, 83 DAS; full pod, R4, 96 DAS; and beginning seed, R5, 111 DAS; Fehr et al., 1971). Following the same timeline, composite soil samples (3 cores) were collected at a 0-to-60 cm soil depth in each plot, near the plant biomass sampling spot, to determine total soil N content (NO_3-N + NH_4^+-N).

Aboveground biomass samples were collected by cutting a 1 m row segment at ground level, resulting in a sample area of 0.76 m^2. Five representative plants were sub-sampled and dried in an air-forced oven at 65 °C until constant weight to further calculate the water content and estimate the dry W. The biomass at the plant level (g $plant^{-1}$) was estimated by dividing the total aboveground dry matter (g) of the sample by the number of plants. In addition, at the first sampling, five extra representative plants were selected for partitioning into lamina (referred to as leaf), stem + petioles (referred to as stem). For subsequent sampling times, three additional representative plants were selected for the same partitioning process to study the leaf-to-stem ratio. Leaf area was measured by passing all individual leaves through a LI-3100 Area Meter (LI-3100, inc., Lincoln, NE) to estimate leaf area index (LAI) and total leaf area.

Samples of dried plants and their components (leaves, stems) were ground and passed through a 250 µm mesh sieve to subsequently determine the N derived from the atmosphere (Ndfa, %) and the %Nc (%) in the plant tissues. Plant N uptake was determined by multiplying the plant biomass by plant %Nc. The Ndfa at each sampling time was determined by the 15N natural abundance method using an isotope mass spectrometer, which measures the excess 15N isotope in soybean compared to a reference plant (Unkovich et al., 2008). The total Ndfa was calculated only for the soybean nodulating genotypes, using the non-nodulating genotypes within their respective block and N rate as the reference plant. The calculation followed Equation 1, with a "B_{value}" of −2.54 as determined by Balboa and Ciampitti (2020) using

$$\text{Ndfa} = \frac{\delta^{15}N_{non-nodulating\ soybean} - \delta^{15}N_{nodulating\ soybean}}{\delta^{15}N_{non-nodulating\ soybean} - B_{value}} x100\ .$$

Statistical analysis

Critical N dilution curve

The critical N dilution curve for the non-nodulating genotypes was described by a relationship between %Nc and biomass (Mg ha^{-1}) (Lemaire et al., 1984), using the Bayesian hierarchical framework described by Lacasa et al. (2023). In the first step, the data model describes the %Nc (N_{ij}) for the i^{th} observation and the j^{th} sampling time, following a normal distribution with expected mean μ_{ij}, and variance σ^2. The μ_{ij} was specified as a non-linear equation, with parameters $A1$ and $A2$. The coefficients *A1* and *A2* describe the $\%N_c$ when plant biomass is equal to 1 Mg ha^{-1} and the magnitude of the dilution. Mathematically this partial component of our hierarchical Bayesian model, described in the text above can be written as:

$$N_{ij} \mid \mu_{ij}, \sigma^2 = Normal\left(\mu_{ij}, \sigma^2\right),$$

$$\mu_{ij} = A1 \cdot W_{max_j}^{-A2},$$

$i = 1, 2, \ldots, 160,$

$j = 1, 2, 3, 4, 5.$

For the second level of our hierarchical Bayesian model, the maximum biomass at each sampling time (W_{max_j}), following a truncated normal distribution with expected value θ_j, and variance τ^2. The expected value θ_j was modeled with a linear-plateau function where W_j was the biomass at the plateau and S_j was the slope for the j^{th} sampling time. Mathematically this component of our hierarchical Bayesian model can be written as:

$$W_{max_j} \mid \theta_j, \tau^2 = Normal(\theta_j, \tau^2)T(0, \infty),$$

$$\theta_j = \begin{cases} W_j + S_j \cdot (N_{ij} - Ncritical_j) & \text{if } N_{ij} < Ncritical_j \\ W_j & \text{otherwise} \end{cases}.$$

To fully specify our hierarchical Bayesian model, we need to set the priors. The slope parameter S_j assumed a truncated normal distribution with expected value μ_s and variance ϕ^2. The prior distribution for *A1* was informed according to previous studies (see Section 2). For A2, a uniform distribution prior from 0 to 1 was specified due to the lack of studies using this two-step model to define crop N dilution in soybeans. A gamma prior distribution was determined for $\sigma^2, \tau^2, and\ \phi^2$ by specifying shape and rate. The parameterization of the gamma distribution expected value and variance was given by $shape/ratio$ and $shape/ratio^2$, respectively:

$$S_j \sim Normal(\mu_s, \phi^2)\mathrm{T}(0, \infty),$$

$$\mu_s \sim Normal(0,10),$$

$$A1 \sim Normal(3.65, 0.24),$$

$$A2 \sim Uniform(0,1),$$

$$\sigma^2, \tau^2, \phi^2 \sim Gamma(0.001, 0.001).$$

For the nodulating soybean genotypes, a Bayesian framework following Almeida et al. (2023) was utilized. The data model assumed a normal distribution for the i^{th} observation of the dependent variable N_i. The data process employed a negative power regression as with the non-nodulating genotypes. However, instead of defining W_{max} for each N_i, all biomass observations were considered in a single step. The same priors as used for the non-nodulating genotypes were employed:

$$N_i \mid \mu_i, \sigma^2 = Normal(\mu_i, \sigma^2),$$

$$\mu_i = A1 \cdot W_{max}^{-A2},$$

$$A1 \sim Normal(3.65, 0.24),$$

$$A2 \sim Uniform(0, 1),$$

$$\sigma^2 \sim Gamma(0.001, 0.001).$$

The statistical models were fitted iteratively at each sampling time with an MCMC algorithm using the *rjags* package (Plummer, 2008).

N uptake, leaf area, leaf weight, biomass and N concentration

The dynamic between pod N uptake and pod biomass, and leaf:stem N uptake and plant biomass were evaluated by linear regression models. The relationship between plant N uptake and plant biomass, leaf N uptake and leaf area, leaf weight and leaf area, soil and atmospheric %Nc and plant biomass were evaluated by non-linear models (a power function $y = \mathrm{a} \cdot x^b$ was employed). All statistical analyses were performed using R statistical software (R Core Team, 2023).

Results

Review: soybean N dilution curves

The synthesis-analysis of existing literature provided valuable information on the range of variation for %Nc when plant biomass is 1 Mg ha^{-1} (A1), with %Nc ranging from 3.02 to 4.36, with an average of 3.65. The dilution parameter that stipulates dilution intensity through time (A2) ranged from -0.066 to -0.163, with an average of -0.115. The maximum plant biomass explored by those experiments ranged from 5 to 13 Mg ha^{-1}, with an average of 7.3 Mg ha^{-1}. Detailed values for these parameters are presented in **Table 3.1,** and the fitted model presented in **Figure 3.1A.**

Table 3.1. Reported parameters for soybean N dilution curves in previous studies (adapted from Santachiara et al., 2018). The A1 parameter refers to plant N concentration at 1 Mg ha^{-1}, and the A2 parameter regulates the intensity of the plant N dilution over time.

Reference	A1	A2	Maximum plant biomass (Mg ha^{-1})
Ney et al. (1997)*	3.02	-0.149	5.1
Salvagiotti et al. (2009)	4.36	-0.156	7.8
Bender et al. (2015)*	3.68	-0.105	6.4
Divito et al. (2016)	3.70	-0.080	8.0
Gaspar et al. (2017)*	2.98	-0.066	6.1
Santachiara et al. (2018)	3.87	-0.163	7.6
Almeida et al. (2023)	3.91	-0.090	13.0
Average	3.65	-0.115	7.7

The nodulating genotypes presented minimum yield variation between 0 and 300 kg ha^{-1} of N (up to 0.5 Mg ha^{-1}), while the non-nodulating genotypes were highly affected by N fertilization, resulting in a difference, for the same N rates, of 1.6 Mg ha^{-1}, on average. The overall plant N dilution was 46% greater in the non-nodulating genotypes (A2 = 0.38) compared to the nodulating counterpart (A2 = 0.26). The estimated %Nc at 1 Mg ha^{-1} (A1) was nearly identical for both genotypes (A1 = 5.0 and 4.9 for non-nodulating and nodulating genotypes,

respectively). For the non-nodulating genotype, the %Nc ranged from 1.1 to 3.8%, while for the nodulating genotype the %Nc varied from 1.9 to 4.1%. The plant biomass ranged from ~2.5 to 12 Mg ha^{-1} for both genotypes. Considering the 95% credible interval of the average dilution curves of both genotypes, differences in %Nc were more evident with plant biomass values above ~3.2 Mg ha^{-1} (**Figure 3.1B**).

Table 3.2. Soybean seed yield, biomass (Mg ha^{-1}) and plant N concentration (%Nc) at varying crop growth stages for all genotypes under different fertilizer N rates.

		Nodulating		Non-nodulating	
	N rate (kg ha^{-1})	nod1	nod2	non_nod1	non_nod2
Grain yield (Mg ha^{-1})	0	2.7	2.4	1.4	1.4
	100	1.8	2.3	1.8	1.6
	200	2.2	2.4	2.9	2.0
	300	2.6	2.9	3.0	3.1
Biomass (Mg ha^{-1}, %Nc) Beginning Bloom, R1	0	2.7 (3.2)	2.5 (3.2)	2.8 (2.5)	2.8 (2.6)
	100	3.0 (3.3)	2.9 (3.5)	3.2 (3.3)	2.9 (3.3)
	200	3.7 (3.6)	3.9 (3.8)	3.7 (3.5)	3.7 (3.7)
	300	3.0 (3.7)	3.5 (3.9)	3.3 (3.6)	2.7 (3.7)
Biomass (Mg ha^{-1}, %Nc) Full Bloom, R2	0	5.8 (3.5)	5.3 (3.2)	4.7 (2.4)	4.8 (2.0)
	100	4.6 (3.3)	5.1 (3.4)	4.9 (3.1)	5.0 (3.1)
	200	4.6 (3.7)	4.9 (3.8)	5.4 (3.6)	4.7 (3.4)
	300	4.3 (3.8)	4.9 (3.8)	4.1 (3.6)	4.7 (3.5)
Biomass (Mg ha^{-1}, %Nc) Beginning Pod Development, R3	0	6.8 (3.6)	6.4 (3.1)	5.7 (2.3)	5.7 (2.2)
	100	5.8 (3.6)	6.1 (3.5)	5.6 (2.8)	6.4 (3.1)
	200	5.7 (3.6)	6.9 (3.4)	7.0 (2.9)	6.3 (3.4)
	300	6.2 (4.1)	5.9 (3.6)	4.6 (3.6)	7.2 (3.8)
Biomass (Mg ha^{-1}, %Nc) Full Pod, R4	0	7.3 (2.7)	7.7 (2.5)	6.6 (1.4)	6.2 (1.5)
	100	7.6 (2.7)	8.0 (2.7)	7.8 (1.9)	7.8 (2.1)
	200	6.8 (2.4)	8.2 (2.7)	9.6 (2.5)	7.8 (2.6)
	300	8.1 (2.9)	8.7 (2.7)	6.8 (2.8)	6.3 (2.9)
Biomass (Mg ha^{-1}, %Nc) Beginning Seed, R5	0	10.0 (2.0)	10.6 (2.1)	8.5 (1.1	7.2 (1.2)
	100	9.8 (2.0)	10.4 (1.9)	11.2 (1.6)	9.5 (1.4)
	200	10.1 (2.1)	9.5 (2.0)	11.1 (2.0)	10.1 (1.7)
	300	11.9 (2.1)	11.2 (2.1)	10.0 (2.1)	11.0 (2.0)

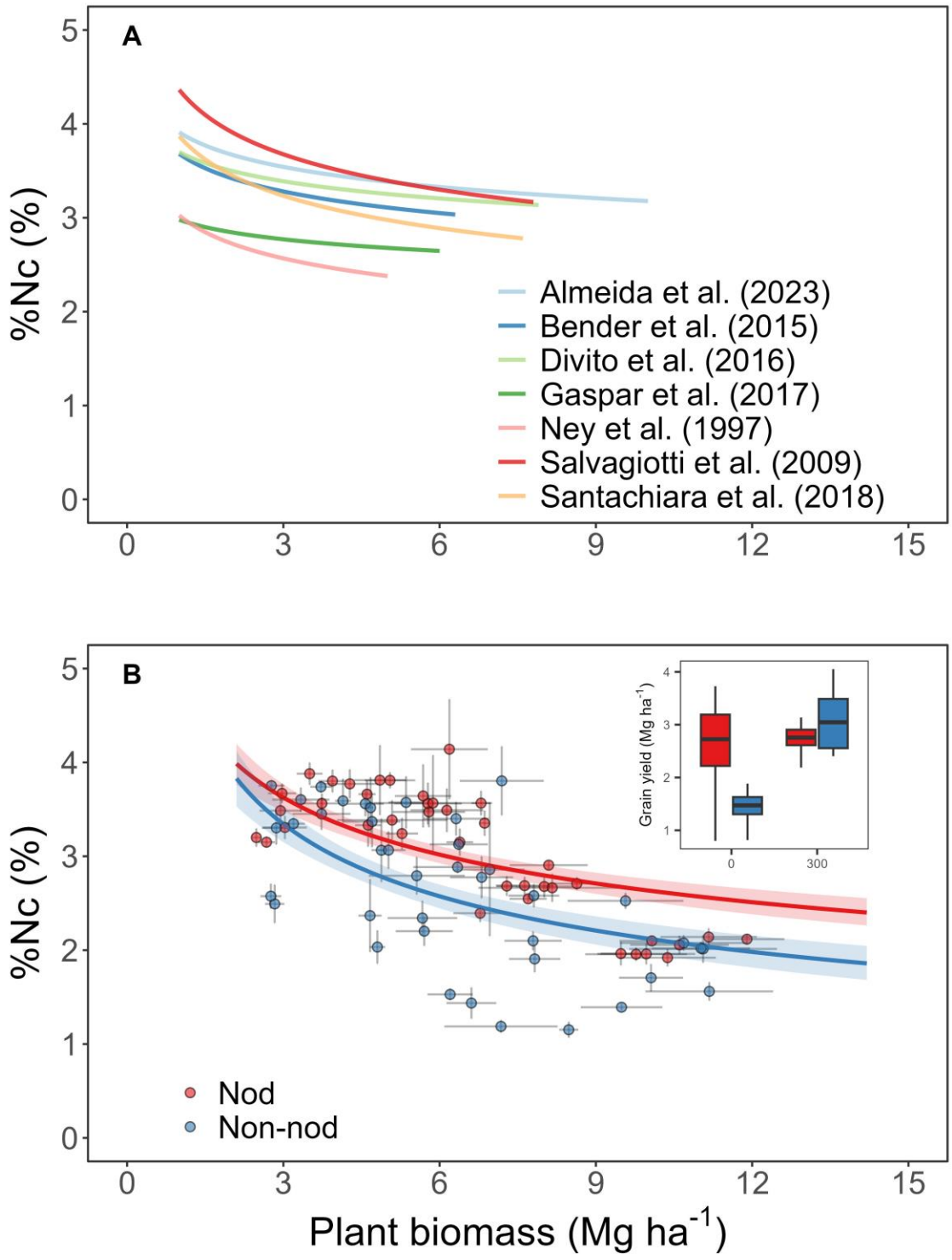


Figure 3.1. Synthesis-analysis of plant N dilution curves for soybeans (A). Relationship between plant N concentration (%Nc) and plant biomass for nodulating (Nod) and non-nodulating (Non-nod) genotypes (B). In B, the red line corresponds to the critical N dilution curve (%N = 4.9 $W^{-0.26}$) adjusted for nodulating genotypes, while the blue line corresponds to the critical N dilution curve adjusted for non-nodulating genotypes (% N = 5.0 $W^{-0.38}$). Those critical dilution curves

were established using the data of all fertilizer N rates, following the guidelines provided by Fernandez et al. (2022). The shaded area corresponds to the 95% credible interval.

Dynamics of plant N distribution and N sources

Both nodulating and non-nodulating genotypes exhibited a diminishing increase in N uptake with increasing biomass leading to a N dilution. The nodulating genotypes presented a 30% slower rate of decline in N uptake with increasing biomass compared to non-nodulating genotypes (exponent parameters of 0.68 and 0.52, respectively). (**Figure 3.2A**). Nodulating genotypes reported 45% greater SLN in comparison to non-nodulating soybeans (1.6 g m^{-2}) (**Figure 3.2B**). Nodulating genotypes exhibited ~20% greater SLA than non-nodulating counterpart (3.21 dm^2 g^{-1} and 2.67 dm^2 g^{-1}, respectively). The SLW was reduced by 17% on the non-nodulating genotypes (0.311 and 0.375 g dm^{-2}, respectively) (**Figure 3.2C**). The N in pods accumulates strictly proportionally to pod biomass, i.e. with no N dilution and then a constant pod N concentration higher for nod plants (4gN/100g) than for non-nod plants (2.5gN/100g) (**Figure 3.3D**). Lastly, there was no significant difference in the leaf: stem N uptake and plant biomass ratios between non-nodulating and nodulating genotypes (**Appendix Figure B.3**).

Soil N dilution was 25% greater in the non-nodulating genotype (A2 = 0.43) relative to the nodulating counterpart (A2 = 0.34). The nodulating genotype resulted in ~0.7% greater %Nc derived from soil N sources compared to the non-nodulating soybean (**Figure 3.3A**). The plant %Nc derived from the atmospheric N fixation process showed an increase throughout the crop growth period in the nodulating soybean genotypes (**Figure 3.3A**). The plant N sourcing revealed a high soil-derived N uptake at the very beginning (0.103 g of N at 1 g of biomass) with a decreasing N uptake rate as the biomass increased (exponent = 0.52). The atmospheric N presented minimum contribution early in the season (0.0015 g of N at 1 g of biomass), and an increasing N uptake rate as biomass increased (exponent = 1.35) (**Figure 3.3B**).

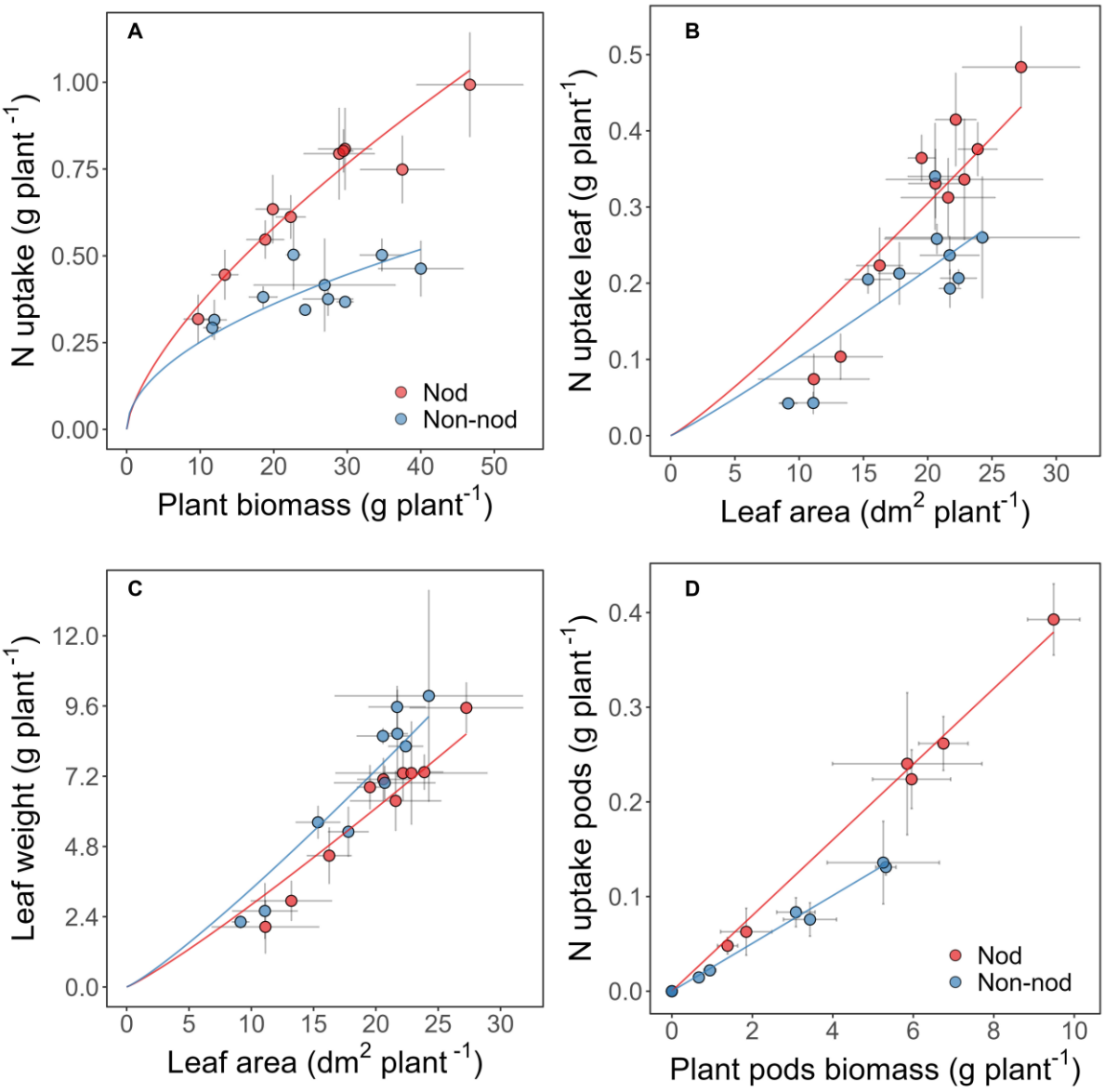


Figure 3.2. Plant nitrogen uptake as a function of aboveground plant biomass (A) for nodulating (Nod) and non-nodulating (Non-nod) genotypes, with nodulating genotypes described by $y = 0.757x^{0.68}$ and non-nodulating genotypes by $y = 0.757x^{0.52}$. Nitrogen uptake on leaves versus leaf area (B) reveals a linear increase that can be described by $y = 0.016x$ and $y = 0.011x$ for nodulating (nod) and non-nodulating (non-nod) genotypes, respectively. Leaf weight relative to leaf area (C) for nodulating (nod, $y = 0.311x$) and non-nodulating (non-nod, $y = 0.375x$) genotypes. Relationship of N uptake (g plant-1) by pods and pods biomass (g plant^{-1}) (D) for nodulating (red) and non-nodulating genotypes (blue). Nodulating are described by $y = 0.04x$, and non-nodulating are described by $y = 0.025x$.

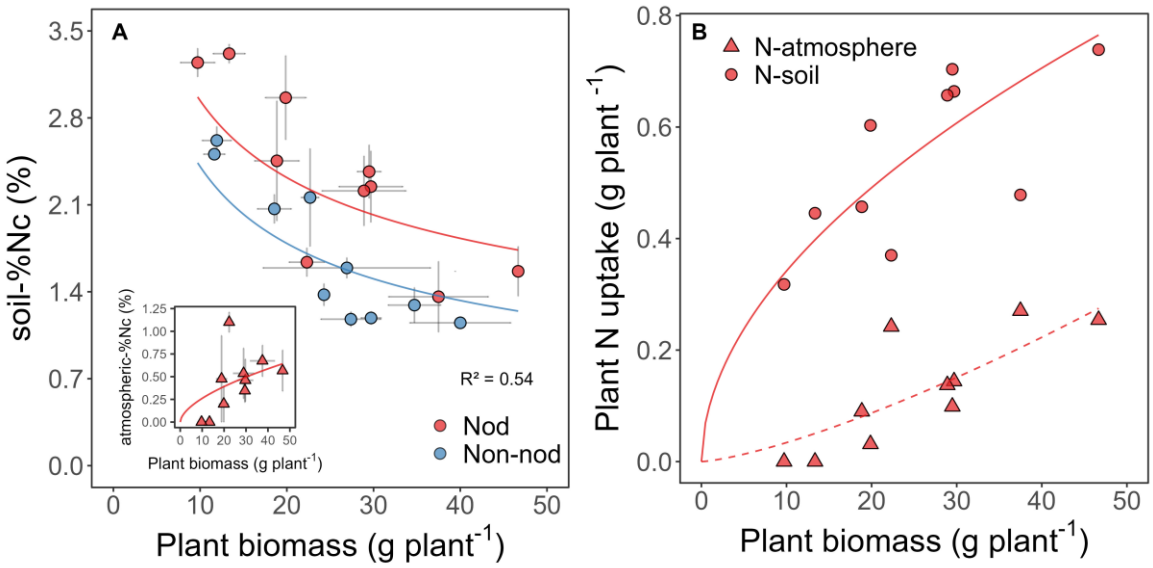


Figure 3.3. Variations in N source utilization across plant biomass levels. The relationship between plant N concentration derived from soil N sources (soil-%Nc, %) and plant biomass (g plant^{-1}) (A) can be described by $y = 6.4564x^{-0.34}$ for the nodulating genotype and by $y = 6.4564x^{-0.43}$ for the non-nodulating genotype. The relationship between plant N concentration derived from the N fixation process (atmospheric-N, %Nc, %) and plant biomass (A) can be described by $y = 0.07x^{0.58}$ for the nodulating genotype. Plant N uptake sourced from soil (circles– solid line) and atmosphere (triangles – dashed line) (C) are described by $y = 0.1030x^{0.52}$ and $y = 0.0015x^{1.35}$. Red symbols and lines correspond to nodulating, and blue corresponds to non-nodulating genotypes.

Discussion

This study provides for the first time, to the extent of our knowledge, a critical N dilution curve for soybean crop using non-nodulating genotypes. Previous studies reporting plant N dilution curves did not properly account for the different crop N sources for soybeans (Almeida et al., 2023; Divito et al., 2016; Ney et al., 1997; Salvagiotti et al., 2008; Santachiara et al., 2018). The N dilution of non-nodulated soybean plants followed a critical curve roughly similar to those of most of the other non-legume C3 species, as shown for many cereals such as maize (*Zea mays* L.), rice (*Oryza sativa* L.), wheat (*Triticum aestivum* L.), and sorghum (*Sorghum bicolor* L.) (Ciampitti et al., 2022). The value of coefficient *A2* (-0.38) is within the range of the values already published for cereal species (see (Ciampitti et al., 2022; Greenwood et al., 1990;

Lemaire et al., 2008)). Nodulated soybean crop showed a less accentuated N dilution as crop mass increased, leading then to a lower value of coefficient *A1* because of the auto-correlation between value of *A1* and *A2* (Makowski et al., 2020). Therefore, it appears that plants having access to both soil mineral N absorption and N_2 fixation were able to increase the intrinsic N capacity (herein understood as more N at similar crop mass), as reflected in leaf, stem, and pods, relative to those soybean plants having only access to soil N resources.

Previous determination of N dilution curves on other legumes such as alfalfa (*Medicago sativa* L.) showed a curve very close to the critical N curve obtained for different grass species (Ciampitti et al., 2022) and to the critical presented here for the non-nodulated soybean. Moreover even when large amounts of N fertilizer are applied, there is no N luxury accumulation and the dilution curve remains unchanged (Lemaire et al. 1992). Thus, the feed-back regulation of N accumulation in relation to plant growth dynamic seems to operate with the same efficiency for root N absoption and N_2-fixation processes as well described in the literature (Briat et al., 2020; Gastal et al., 2015). A similar N-feedback mechanism has been reported for other legumes (Shulze et al., 2003), with delayed N senescence prolonging the N_2-fixation activity (Abu-Shakra et al., 1978). However, in annual grain legumes such as soybeans that present a high N demand (high protein values), the ability of the plant to accumulate more N per unit of biomass is needed to satisfy this additional N requirement. The comparison of nodulated versus non-nodulated soybeans clearly highlights that soybean plants relying on N_2-fixation activity can accumulate more N per unit of biomass, increasing the intrinsic N capacity.

From a crop physiological standpoint, soybeans are well known for storing high quantity of N in different vegetative organs (Staswick, 1990) for satisfying nutritional needs during the last phases of the reproductive period. A temporary storage of N as the vegetative storage protein

(VSP) is usually regulated based on the stored surplus N. The VPS, first characterized by Wittenbach (1983), with a dynamic of increasing with N supply and then declining during the seed-filling period. These proteins are found in leaves, stems, and pod tissues, as a primary temporary reservoir of N in young seed pods (Staswick, 1989), regulated based on the plant N status (acting both as sink or sources). Under N deficiency, the VSP expression is negligible (Staswick, 1990). Increases in plant N status via VSP accumulation in vacuoles might avoid the down recirculation of N to root through phloem as a signal of N satisfaction for feedback repressing N_2 fixation. During the late reproductive season, when seed N demand is not met due to new N uptake and/or N fixation (Thibodeau and Jaworski, 1975), the N remobilization process will start to meet this deficit (Borst and Thatrther, 1931; Sinclair and de Wit, 1975, 1976). In a recent study, Ortez et al. (2019) quantified the main sources of N contribution to seeds, with more than 50% derived from leaf organs, 30% from pods, and the remaining N from the stem tissue. The leaf organ, due to the intrinsic capacity to store N and metabolic N, is the major tissue contributing to seed N demand (Devries et al., 1989) via the remobilization process.

It is noteworthy to emphasize that for perennial legumes such as alfalfa, VSP accumulates on tap root parenchyma as N reserves for sustaining plant regrowth after defoliation and/or after winter (Kim et al. 1991; Avice et al. 1997; Avice et al. 1996). Therefore, perennial species variations due to the use and replenishment of VSP reserves in tap root during the plant regrowth process are not taken into account in the N dilution curves based on shoot biomass accumulation as well demonstrated in Lemaire et al. 1992. Partially, the difference in N dilution curves between alfalfa and soybean might be due to the localization of the VSP reserves either in tap root or in other vegetative structures such as in leaf, stem, and pods, but in both cases, VSP accumulation is a mechanism for plant to store N reserves by sequestrating luxury N, avoiding

then the N feed-back regulation of both N mineral absorption and N_2-fixation linked with the down recirculation of luxury N through phloem sap (Fujita et al., 1991; Schulze, 2003).

Future research should focus on understanding the environmental drivers affecting the critical N dilution curve in soybeans utilizing non-nodulating genotypes. Breeding programs should prioritize the development of non-nodulating isolines to facilitate N dilution studies and the identification of traits that enhance the effective use of N from both soil and N_2-fixation processes. This study represents a significant step towards the more accurate utilization of diagnostic tools, such as the Nitrogen Nutrition Index (NNI), for assessing N status in soybeans and potentially improving both yield and seed quality.

Conclusions

This study established a critical N dilution curve in soybeans using non-nodulating genotypes, revealing a greater dilution relative to the one for nodulating soybean varieties previously reported in the scientific literature. In addition, this research underscored the major role of the N reservoir in improving light interception (increasing specific leaf area) and attaining high N content in nodulating soybeans.

References

A. Almeida, L.F., Correndo, A., Ross, J., Licht, M., Casteel, S., Singh, M., Naeve, S., Vann, R., Bais, J., Kandel, H., Lindsey, L., Conley, S., Kleinjan, J., Kovács, P., Dan Berning, Hefley, T., Reiter, M., Holshouser, D., Ciampitti, I.A., 2023. Soybean yield response to nitrogen and sulfur fertilization in the United States: contribution of soil N and N fixation processes. European Journal of Agronomy 145, 126791. https://doi.org/10.1016/j.eja.2023.126791

Balboa, G.R., Ciampitti, I.A., 2020. Estimating biological nitrogen fixation in field-grown soybeans: impact of B value. Plant Soil 446, 195–210. https://doi.org/10.1007/s11104-019-04317-1

Bender, R.R., Haegele, J.W., Below, F.E., 2015. Nutrient Uptake, Partitioning, and Remobilization in Modern Soybean Varieties. Agronomy Journal 107, 563–573. https://doi.org/10.2134/agronj14.0435

Briat, J.-F., Gojon, A., Plassard, C., Rouached, H., Lemaire, G., 2020. Reappraisal of the central role of soil nutrient availability in nutrient management in light of recent advances in plant nutrition at crop and molecular levels. European Journal of Agronomy 116, 126069. https://doi.org/10.1016/j.eja.2020.126069

Ciampitti, I., van Versendaal, E., Rybecky, J.F., Lacasa, J., Fernandez, J., Makowski, D., Lemaire, G., 2022. A global dataset to parametrize critical nitrogen dilution curves for major crop species. Sci Data 9, 277. https://doi.org/10.1038/s41597-022-01395-2

Divito, G.A., Echeverría, H.E., Andrade, F.H., Sadras, V.O., 2016. Soybean shows an attenuated nitrogen dilution curve irrespective of maturity group and sowing date. Field Crops Research 186, 1–9. https://doi.org/10.1016/j.fcr.2015.11.004

Evans, J.R., 1989. Photosynthesis and nitrogen relationships in leaves of C3 plants. Oecologia 78, 9–19. https://doi.org/10.1007/BF00377192

Fehr, W.R., Caviness, C.E., Burmood, D.T., Pennington, J.S., 1971. Stage of Development Descriptions for Soybeans, Glycine Max (L.) Merrill1. Crop Science 11, cropsci1971.0011183X001100060051x. https://doi.org/10.2135/cropsci1971.0011183X001100060051x

Fernandez, J.A., van Versendaal, E., Lacasa, J., Makowski, D., Lemaire, G., Ciampitti, I.A., 2022. Dataset characteristics for the determination of critical nitrogen dilution curves: From past to new guidelines. European Journal of Agronomy 139, 126568. https://doi.org/10.1016/j.eja.2022.126568

Fujita, K., Masuda, T., Ogata, S., 1991. Analysis of factors controlling dinitrogen fixation in wild and cultivated soybean (Glycine max) plants by reciprocal grafting. Soil Science and Plant Nutrition 37, 233–240. https://doi.org/10.1080/00380768.1991.10415033

Gaspar, A.P., Laboski, C.A.M., Naeve, S.L., Conley, S.P., 2017. Dry Matter and Nitrogen Uptake, Partitioning, and Removal across a Wide Range of Soybean Seed Yield Levels. Crop Science 57, 2170–2182. https://doi.org/10.2135/cropsci2016.05.0322

Gastal, F., Lemaire, G., Durand, J.-L., Louarn, G., 2015. Quantifying crop responses to nitrogen and avenues to improve nitrogen-use efficiency.

GREENWOOD, D.J., LEMAIRE, G., GOSSE, G., CRUZ, P., DRAYCOTT, A., NEETESON, J.J., 1990. Decline in Percentage N of C3 and C4 Crops with Increasing Plant Mass. Annals of Botany 66, 425–436. https://doi.org/10.1093/oxfordjournals.aob.a088044

Grindlay, D.J.C., 1997. REVIEW Towards an explanation of crop nitrogen demand based on the optimization of leaf nitrogen per unit leaf area. The Journal of Agricultural Science 128, 377–396. https://doi.org/10.1017/S0021859697004310

Jones Jr., J.B., Case, V.W., 1990. Sampling, Handling, and Analyzing Plant Tissue Samples, in: Soil Testing and Plant Analysis. John Wiley & Sons, Ltd, pp. 389–427. https://doi.org/10.2136/sssabookser3.3ed.c15

Justes, E., Mary, B., Meynard, J.-M., Machet, J.-M., Thelier-Huche, L., 1994. Determination of a Critical Nitrogen Dilution Curve for Winter Wheat Crops. Annals of Botany 74, 397–407. https://doi.org/10.1006/anbo.1994.1133

Kottek, M., Grieser, J., Beck, C., Rudolf, B., Rubel, F., 2006. World Map of the Köppen-Geiger climate classification updated. metz 15, 259–263. https://doi.org/10.1127/0941-2948/2006/0130

Lacasa, J., Makowski, D., Hefley, T., Fernandez, J., van Versendaal, E., Lemaire, G., Ciampitti, I., 2023. Comparison of statistical methods to fit critical nitrogen dilution curves. European Journal of Agronomy 145, 126770. https://doi.org/10.1016/j.eja.2023.126770

Lemaire, G., Jeuffroy, M.-H., Gastal, F., 2008. Diagnosis tool for plant and crop N status in vegetative stage: Theory and practices for crop N management. European Journal of Agronomy 28, 614–624. https://doi.org/10.1016/j.eja.2008.01.005

Lemaire, G., Salette, J., Sigogne, M., Terrasson, J.-P., 1984. Relation entre dynamique de croissance et dynamique de prélèvement d'azote pour un peuplement de graminées fourragères. I. — Etude de l'effet du milieu. Agronomie 4, 423–430. https://doi.org/10.1051/agro:19840503

Makowski, D., Zhao, B., Ata-Ul-Karim, S.T., Lemaire, G., 2020. Analyzing uncertainty in critical nitrogen dilution curves. European Journal of Agronomy 118, 126076. https://doi.org/10.1016/j.eja.2020.126076

Ney, B., Dore, T., Sagan, M., 1997. Grain Legumes, in: Lemaire, G. (Ed.), Diagnosis of the Nitrogen Status in Crops. Springer, Berlin, Heidelberg, pp. 107–117. https://doi.org/10.1007/978-3-642-60684-7_6

Nitrogen Fixation and Delayed Leaf Senescence in Soybeans | Science [WWW Document], n.d. URL https://www.science.org/doi/abs/10.1126/science.199.4332.973 (accessed 9.2.24).

Plénet, D., Lemaire, G., 1999. Relationships between dynamics of nitrogen uptake and dry matter accumulation in maize crops. Determination of critical N concentration. Plant and Soil 216, 65–82. https://doi.org/10.1023/A:1004783431055

Plummer, M., 2008. rjags: Bayesian Graphical Models using MCMC. https://doi.org/10.32614/CRAN.package.rjags

Salvagiotti, F., Cassman, K.G., Specht, J.E., Walters, D.T., Weiss, A., Dobermann, A., 2008. Nitrogen uptake, fixation and response to fertilizer N in soybeans: A review. Field Crops Research 108, 1–13. https://doi.org/10.1016/j.fcr.2008.03.001

Santachiara, G., Salvagiotti, F., Gerde, J.A., Rotundo, J.L., 2018. Does biological nitrogen fixation modify soybean nitrogen dilution curves? Field Crops Research 223, 171–178. https://doi.org/10.1016/j.fcr.2018.04.001

Schulze, J., 2003. Source-sink manipulations suggest an N-feedback mechanism for the drop in N2 fixation during pod-filling in pea and broad bean. Journal of Plant Physiology 160, 531–537. https://doi.org/10.1078/0176-1617-00709

Sinclair, T.R., Horie, T., 1989. Leaf Nitrogen, Photosynthesis, and Crop Radiation Use Efficiency: A Review. Crop Science 29, cropsci1989.0011183X002900010023x. https://doi.org/10.2135/cropsci1989.0011183X002900010023x

Staswick, P.E., 1990. Novel Regulation of Vegetative Storage Protein Genes. The Plant Cell 2, 1–6. https://doi.org/10.1105/tpc.2.1.1

Vos, J., Putten, P.E.L. van der, Birch, C.J., 2005. Effect of nitrogen supply on leaf appearance, leaf growth, leaf nitrogen economy and photosynthetic capacity in maize (*Zea mays* L.). Field Crops Research 93, 64–73. https://doi.org/10.1016/j.fcr.2004.09.013

Chapter 4 - Limitations and Future Fesearch

The Chapter 2 provided new insights to improve soybean resilience to climate uncertainties by integrating long-term weather data with crop modeling to identify regional patterns of water stress (WS) and inform soybean management decisions across El Niño Southern Oscillation (ENSO) phases in Southern Brazil. Crop water deficits significantly reduce yields, with potential losses of up to 2 Mg ha^{-1}. The early and intermediate planting dates (October 20th and December 5th) demonstrated favorable outcomes due to increased radiation. However, those planting dates were also linked to greater failure risks during La Niña phases, particularly in the southernmost region. Region-specific strategies are necessary due to climatic variability, with longer maturity groups reducing failure risk by 15% during La Niña in the south. By addressing these challenges and considering planting date, genotype maturity, and ENSO phase interactions, predictive tools can enhance soybean resilience and productivity in water-stressed regions. This ultimately mitigates yield penalties and improves agricultural decision-making.

The Chapter 3 contributed to the understanding of nitrogen (N) dynamics for soybean crop. The utilization of the non-nodulating soybeans revealed greater plant N dilution with increasing biomass relative to the nodulating genotypes. This study provides the first critical N dilution curve for soybeans using non-nodulating genotypes, addressing a knowledge gap in previous studies that failed to account for differential N sources (mainly the effect of N fixation) in soybean crops. Additionally, it also underscores the potential role of vegetative storage proteins in N accumulation and remobilization for sustaining seed N demand. Furthermore, it sheds light on the importance of N reservoirs in improving light interception and achieving high N content in nodulating soybeans.

Although the research makes a substantial contribution to the field, there are new potential avenues for future investigation. A significant limitation of Chapter 2 is the absence of calibration of crop genetic parameters, such as plant biomass and leaf area index, which could refine our understanding of yield formation beyond final products. Additionally, genotype variability within maturity groups, influenced by traits such as root disease susceptibility and stress tolerance, were not considered. Future research should focus on the genetic basis of stress tolerance and develop predictive platforms to refine climate-driven management strategies accounting for the seasonal variability of the sea surface temperature anomalies.

In the context of N management, for Chapter 3, future research is needed to better understand the environmental drivers influencing the critical N dilution curve in soybeans. Breeding programs should continue investing in the development of more non-nodulating isolines to facilitate N dilution studies and the identification of new plant traits that enhance the effective use of N (more N per unit of biomass) from both N sources, soil and N_2-fixation processes. This study represents a significant step towards more accurately utilizing diagnostic tools, such as the Nitrogen Nutrition Index (NNI), for the assesment of soybean N status. By establishing a connection between N management and stress resilience, this work establishes a foundation for the advancement of more sustainable and productive soybean production in an increasingly variable climate.

Appendix A - Chapter 2

Appendix Table A.1. Validation dataset description.

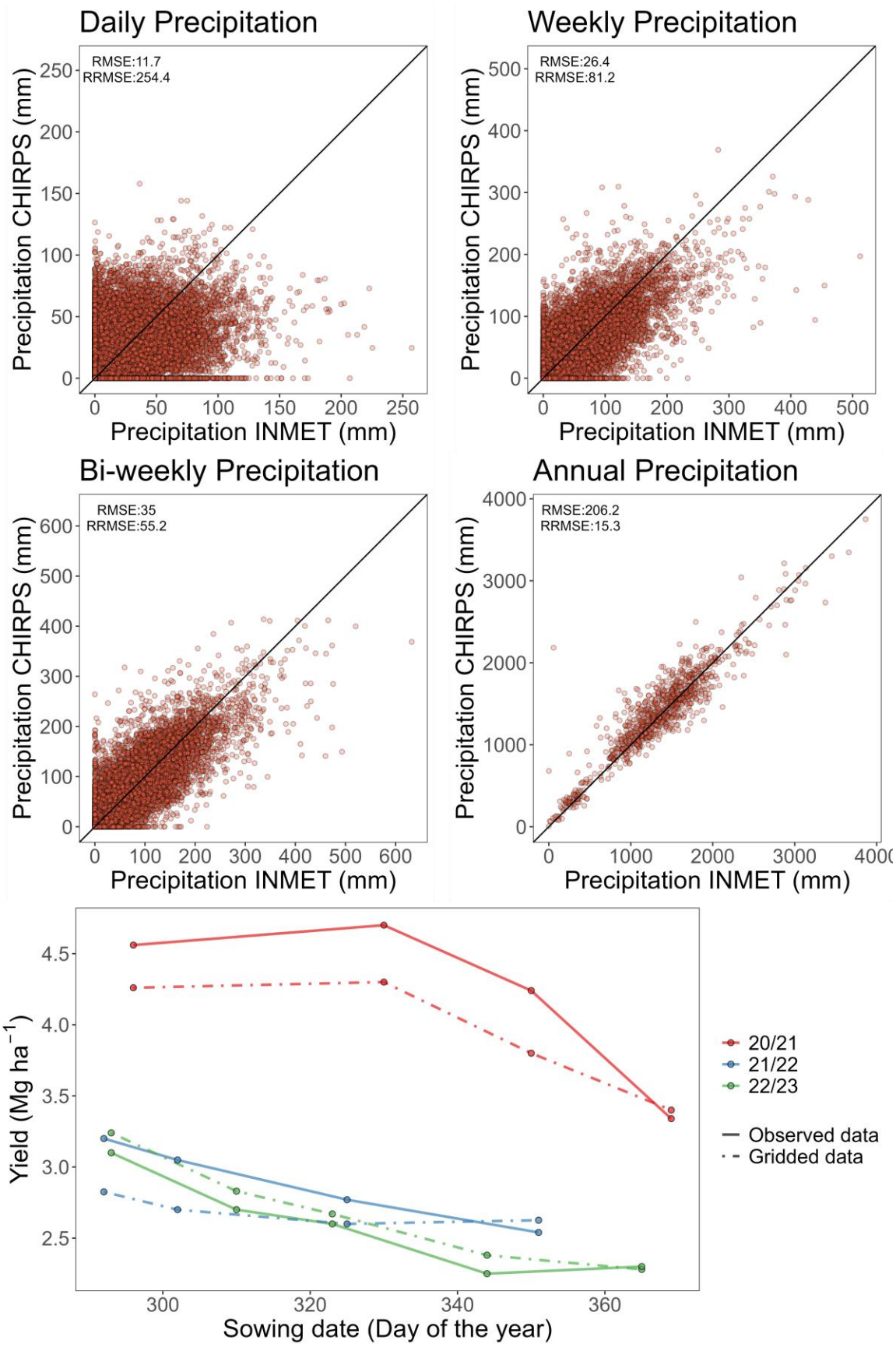
Site	MG	Season	Planting date	Yield
Bagé	5.0	2013/2014 - 2020/2021	08-Nov - 18-Dec	2102 - 5579 (3811)
Bagé	5.8	2013/2014 - 2020/2021	08-Nov - 18-Dec	1569 - 6146 (3635)
Bagé	6.4	2013/2014 - 2020/2021	08-Nov - 18-Dec	1309 - 6394 (3578)
Bagé*	5.0	2013/2014 - 2020/2021	28-Nov - 28-Nov	3358 - 3814 (3586)
Bagé*	5.8	2013/2014 - 2020/2021	28-Nov - 28-Nov	2231 - 4906 (3596)
Bagé*	6.4	2013/2014 - 2020/2021	28-Nov - 28-Nov	2473 - 4845 (3713)
Cacequi	5.0	2013/2014 - 2020/2021	21-Oct - 21-Oct	2361 - 3168 (2715)
Cacequi	5.8	2013/2014 - 2020/2021	21-Oct - 21-Oct	2669 - 4578 (3953)
Cacequi	6.4	2013/2014 - 2020/2021	21-Oct - 21-Oct	3793 - 5388 (4704)
Cachoeira do Sul	5.0	2013/2014 - 2020/2021	08-Nov - 11-Dec	2340 - 5906 (4225)
Cachoeira do Sul	5.8	2013/2014 - 2020/2021	05-Nov - 11-Dec	1671 - 7635 (4580)
Cachoeira do Sul	6.4	2013/2014 - 2020/2021	01-Nov - 11-Dec	1265 - 8363 (4438)
Cachoeira do Sul*	5.0	2013/2014 - 2020/2021	21-Nov - 12-Dec	3139 - 5925 (4674)
Cachoeira do Sul*	5.8	2013/2014 - 2020/2021	21-Nov - 12-Dec	3329 - 6684 (4859)
Cachoeira do Sul*	6.4	2013/2014 - 2020/2021	21-Nov - 12-Dec	3131 - 6411 (4881)
Cruz Alta	5.0	2013/2014 - 2020/2021	25-Nov - 25-Nov	2568 - 3217 (2857)
Cruz Alta	5.8	2013/2014 - 2020/2021	25-Nov - 26-Nov	2974 - 6514 (3917)
Cruz Alta	6.4	2013/2014 - 2020/2021	25-Nov - 26-Nov	3098 - 6822 (4476)
Dom Pedrito	5.0	2013/2014 - 2020/2021	18-Nov - 01-Dec	2462 - 4264 (3623)
Dom Pedrito	5.8	2013/2014 - 2020/2021	18-Nov - 01-Dec	2085 - 5340 (3735)
Dom Pedrito	6.4	2013/2014 - 2020/2021	18-Nov - 01-Dec	1810 - 5598 (4071)
Dom Pedrito*	5.0	2013/2014 - 2020/2021	26-Nov - 26-Nov	3145 - 4744 (3744)
Dom Pedrito*	5.8	2013/2014 - 2020/2021	26-Nov - 26-Nov	2467 - 4397 (3634)
Dom Pedrito*	6.4	2013/2014 - 2020/2021	26-Nov - 26-Nov	2596 - 4748 (3653)
Julio de Castilhos	5.0	2013/2014 - 2020/2021	23-Oct - 14-Nov	3625 - 5284 (4358)
Julio de Castilhos	5.8	2013/2014 - 2020/2021	23-Oct - 14-Nov	3197 - 5940 (4523)
Julio de Castilhos	6.4	2013/2014 - 2020/2021	23-Oct - 14-Nov	3143 - 6032 (4658)
Lagoa Vermelha	5.0	2013/2014 - 2020/2021	04-Nov - 26-Nov	4088 - 4813 (4525)
Lagoa Vermelha	5.8	2013/2014 - 2020/2021	04-Nov - 26-Nov	3079 - 5949 (4731)
Lagoa Vermelha	6.4	2013/2014 - 2020/2021	04-Nov - 26-Nov	3777 - 5610 (4714)
Manoel Viana	5.0	2013/2014 - 2020/2021	23-Nov - 10-Dec	1755 - 5296 (3322)
Manoel Viana	5.8	2013/2014 - 2020/2021	30-Oct - 10-Dec	998 - 6873 (3652)
Manoel Viana	6.4	2013/2014 - 2020/2021	30-Oct - 10-Dec	1376 - 6681 (3853)
Não-Me-Toque	5.0	2013/2014 - 2020/2021	29-Oct - 07-Dec	3549 - 5314 (4412)
Não-Me-Toque	5.8	2013/2014 - 2020/2021	29-Oct - 07-Dec	3575 - 6371 (4899)
Não-Me-Toque	6.4	2013/2014 - 2020/2021	29-Oct - 07-Dec	2443 - 6667 (4814)
Passo Fundo	5.0	2013/2014 - 2020/2021	22-Oct - 16-Dec	2212 - 6043 (4259)

Passo Fundo	5.8	2013/2014 - 2020/2021	22-Oct - 16-Dec	1687 - 7200 (4533)
Passo Fundo	6.4	2013/2014 - 2020/2021	22-Oct - 16-Dec	1327 - 6528 (4381)
Pelotas	5.0	2013/2014 - 2020/2021	13-Nov - 13-Nov	3481 - 5174 (4507)
Pelotas	5.8	2013/2014 - 2020/2021	13-Nov - 13-Nov	4216 - 7339 (6018)
Pelotas	6.4	2013/2014 - 2020/2021	13-Nov - 13-Nov	4318 - 6761 (5478)
Santo Augusto	5.0	2013/2014 - 2020/2021	30-Oct - 26-Jan	1253 - 6501 (4119)
Santo Augusto	5.8	2013/2014 - 2020/2021	30-Oct - 26-Jan	1232 - 7471 (4601)
Santo Augusto	6.4	2013/2014 - 2020/2021	30-Oct - 26-Jan	928 - 7300 (4185)
São Gabriel	5.0	2013/2014 - 2020/2021	04-Nov - 11-Dec	2194 - 6567 (4310)
São Gabriel	5.8	2013/2014 - 2020/2021	25-Sep - 11-Dec	1399 - 6373 (4162)
São Gabriel	6.4	2013/2014 - 2020/2021	25-Sep - 11-Dec	1727 - 6562 (4198)
São Luiz Gonzaga	5.0	2013/2014 - 2020/2021	24-Oct - 16-Dec	1536 - 5948 (4170)
São Luiz Gonzaga	5.8	2013/2014 - 2020/2021	24-Oct - 16-Dec	1667 - 6915 (4516)
São Luiz Gonzaga	6.4	2013/2014 - 2020/2021	24-Oct - 16-Dec	2421 - 7070 (4624)
Tupanciretã	5.0	2013/2014 - 2020/2021	29-Oct - 29-Oct	5509 - 6383 (5946)
Tupanciretã	5.8	2013/2014 - 2020/2021	29-Oct - 29-Oct	5549 - 6769 (6008)
Tupanciretã	6.4	2013/2014 - 2020/2021	29-Oct - 29-Oct	4703 - 6429 (5646)
Vacaria	5.0	2013/2014 - 2020/2021	31-Oct - 18-Dec	2143 - 6269 (4485)
Vacaria	5.8	2013/2014 - 2020/2021	31-Oct - 18-Dec	1195 - 7016 (4663)
Vacaria	6.4	2013/2014 - 2020/2021	31-Oct - 18-Dec	998 - 6633 (4283)

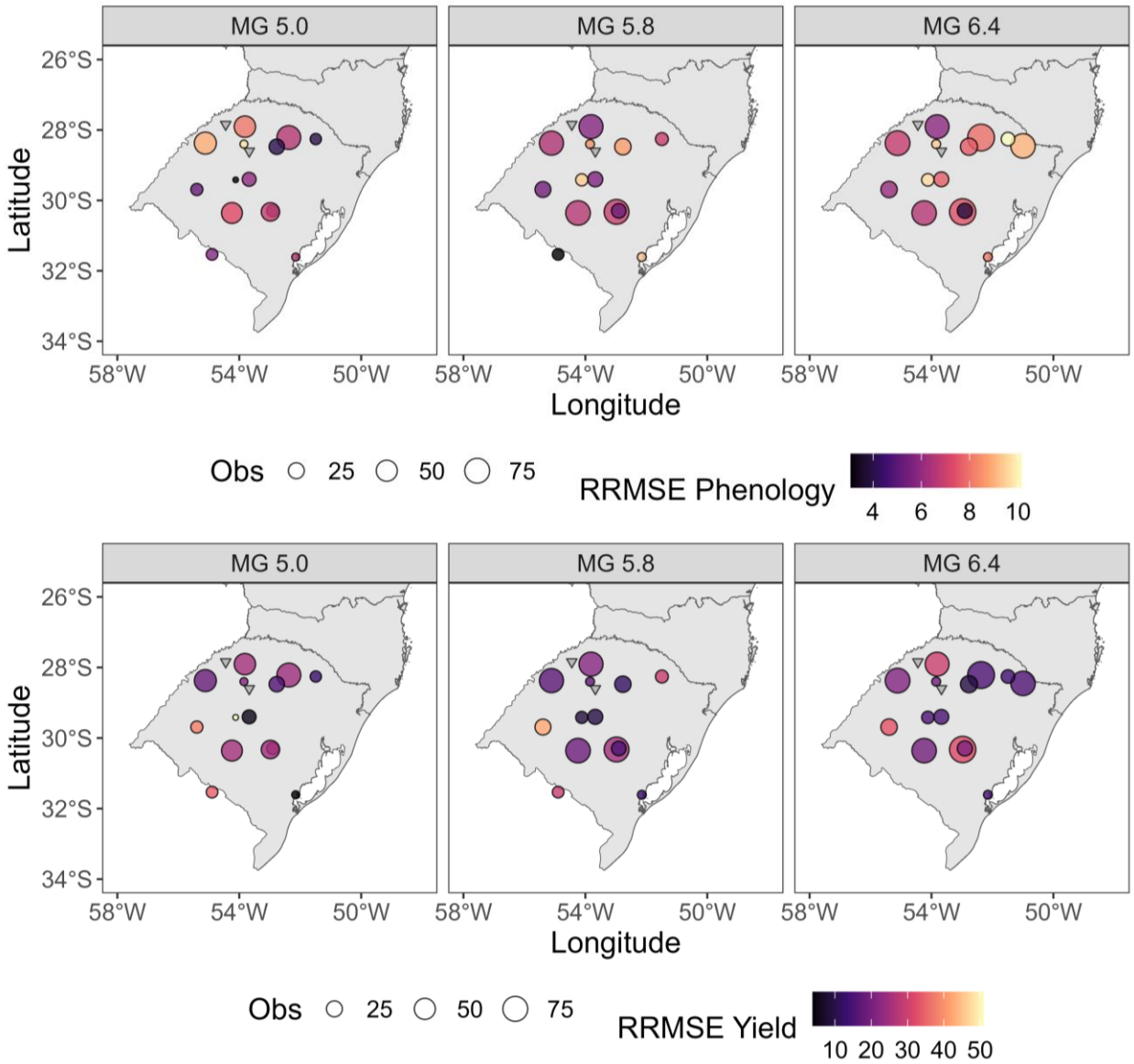
Appendix Table A.2. APSIM Next Generation phenology parameters.

Maturity group	Parameter	Value
5.0	Vegetative.Target.FixedValue	303.7
	EarlyFlowering.Target.FixedValue	261.3
	EarlyGrainFilling.Target.FractionofGrainfilling.FixedValue	0.34
	LateGrainFilling.Target.EntireGrainfillPeriod.FixedValue	415.3
	ReproductivePhotoperiodModifier.XYPairs.X	11.8, 14.2
	VegetativePhotoperiodModifier.XYPairs.X	13.5, 15.0
5.8	Vegetative.Target.FixedValue	558.7
	EarlyFlowering.Target.FixedValue	238.8
	EarlyGrainFilling.Target.FractionofGrainfilling.FixedValue	0.3
	LateGrainFilling.Target.EntireGrainfillPeriod.FixedValue	510.7

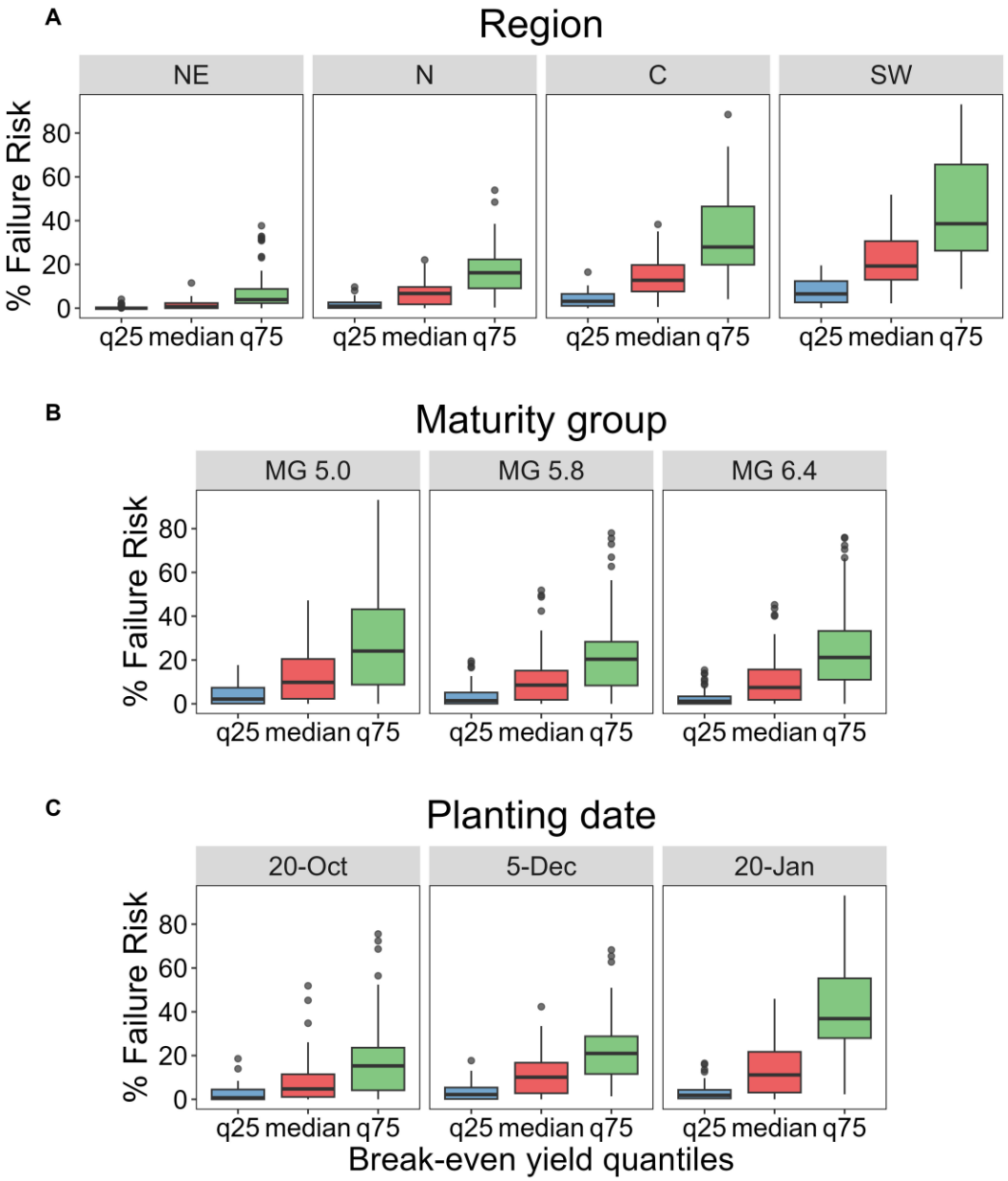
	ReproductivePhotoperiodModifier.XYPairs.X	13.1, 18.3
	VegetativePhotoperiodModifier.XYPairs.X	14.9, 19.8
6.4	Vegetative.Target.FixedValue	594
	EarlyFlowering.Target.FixedValue	281.1
	EarlyGrainFilling.Target.FractionofGrainfilling.FixedValue	0.31
	LateGrainFilling.Target.EntireGrainfillPeriod.FixedValue	450.6
	ReproductivePhotoperiodModifier.XYPairs.X	11.9, 21.2
	VegetativePhotoperiodModifier.XYPairs.X	14.6, 20.0


Daily Precipitation
RMSE:11.7
RRMSE:254.4
Precipitation CHIRPS (mm)
Precipitation INMET (mm)
Weekly Precipitation
RMSE:26.4
RRMSE:81.2
Precipitation CHIRPS (mm)
Precipitation INMET (mm)
Bi-weekly Precipitation
RMSE:35
RRMSE:55.2
Precipitation CHIRPS (mm)
Precipitation INMET (mm)
Annual Precipitation
RMSE:206.2
RRMSE:15.3
Precipitation CHIRPS (mm)
Precipitation INMET (mm)
Yield (Mg ha^{-1})
Sowing date (Day of the year)
20/21
21/22
22/23
Observed data
Gridded data

Appendix Figure A.1. Comparison of observed weather data (INMET – National Meteorology Institute) and gridded weather data (CHIRPS). The bottom panel illustrates an example of the soybean simulated grain yield utilizing observed (solid lines) and gridded (dashed lines) weather data in contrasting seasons.

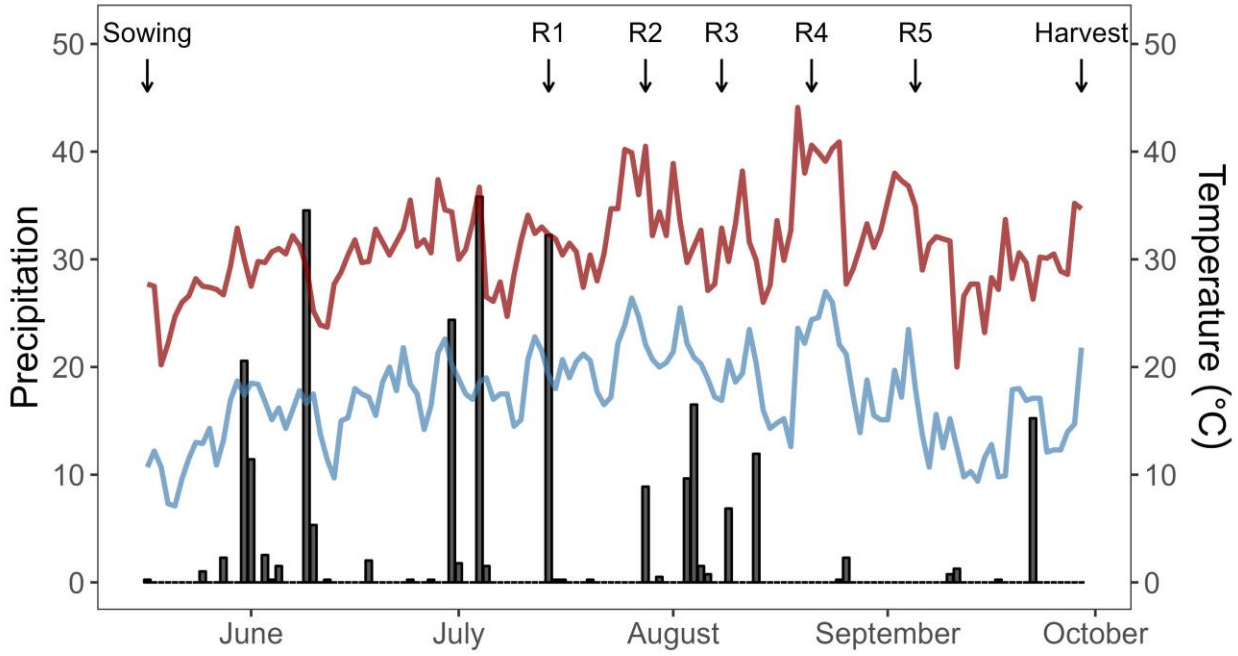


Appendix Figure A.2. Sites utilized for validation (circles) and calibration (triangles). Colors indicate the Relative Root Mean Square Error (RRMSE), and circle size indicates the number of observations at each validation site.

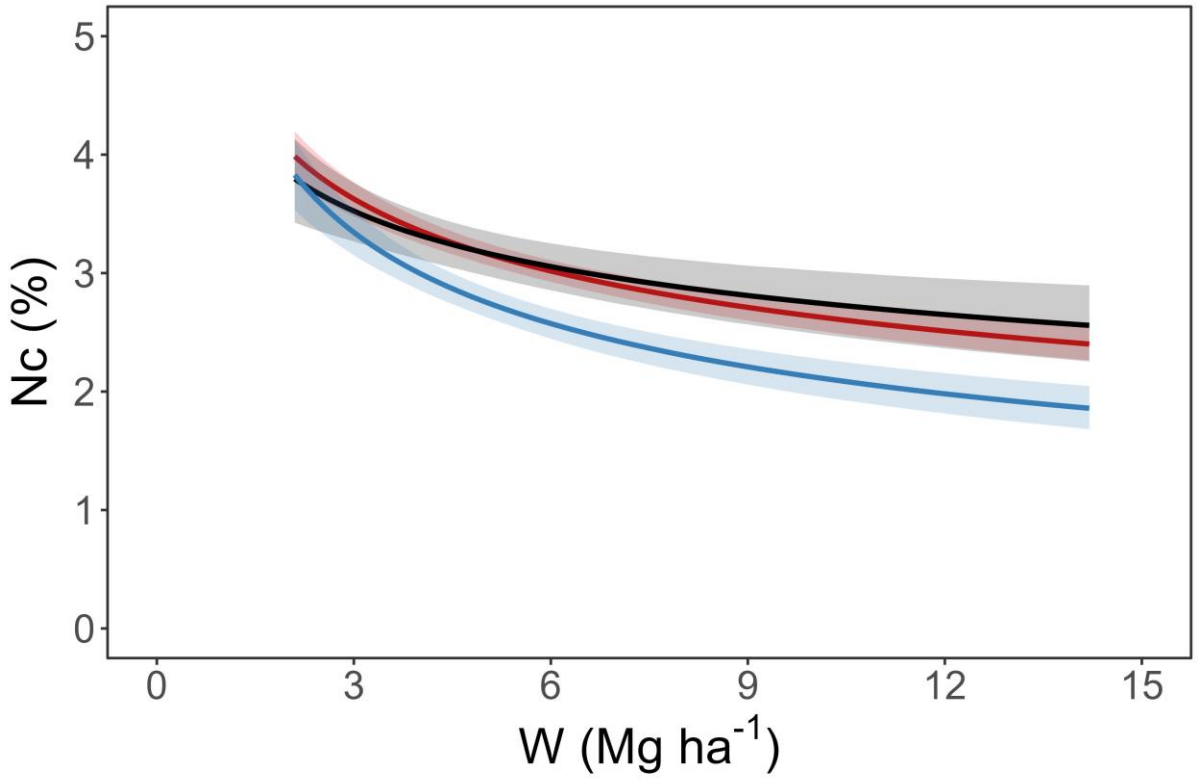


Appendix Figure A.3. Sensitivity analysis of economic break-even yield impact on crop failure risk (%). Quantiles q25 = 1.5 Mg ha^{-1}, median = 2.0 Mg ha^{-1}, and q75 = 2.6 Mg ha^{-1}.

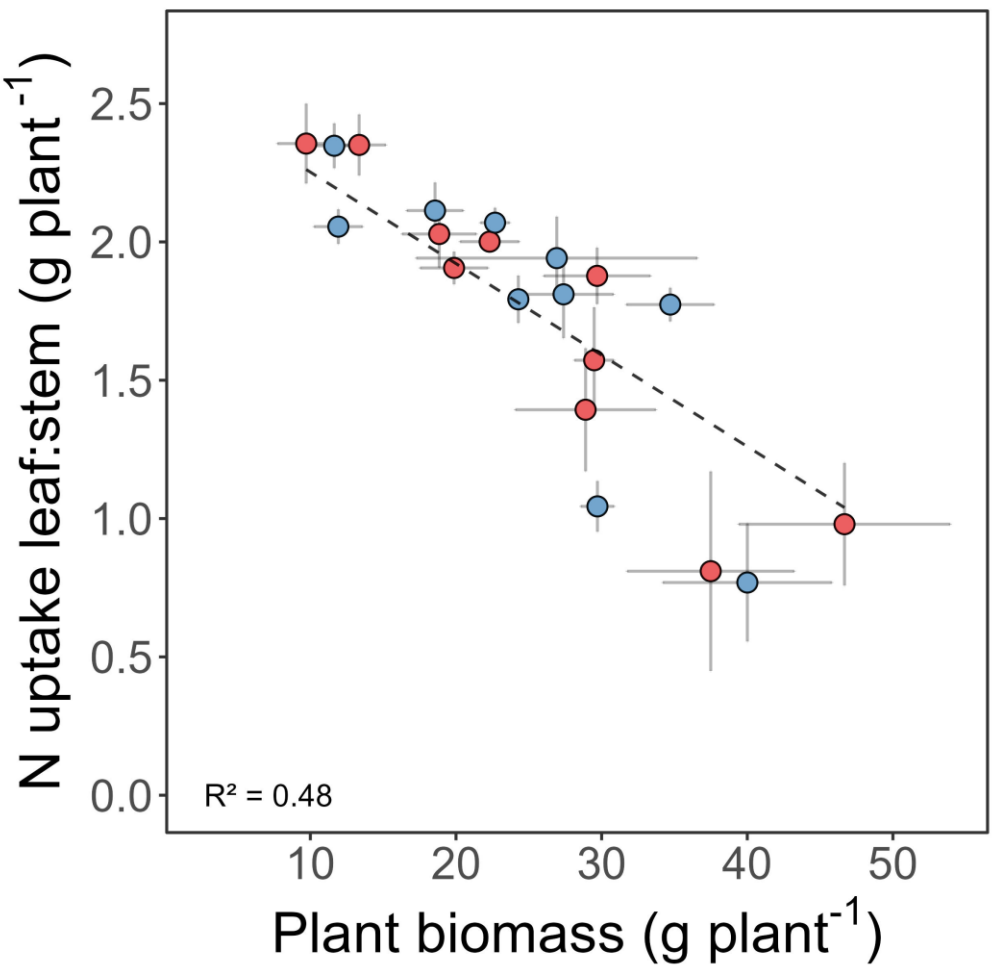
Appendix B - Chapter 3



Appendix Figure B.1. In-season weather characterization: maximum (red) and minimum (blue) temperatures, and precipitation (black bars). Sampling times, sowing, and harvest are illustrated.



Appendix Figure B.2. Comparison of non-nodulating genotypes under no N limitation (300 kg N) curve (black) with the curves presented in Figure 3.1.



Appendix Figure B.3. The relationship between plant aboveground biomass and leaf/stem N ratio was the same for both genotypes and can be described by y = 2.5575 − 0.0332x. Red symbols and lines correspond to nodulating genotypes, blue symbols and lines correspond to non-nodulating genotypes.

Appendix Table B.1. Experiment soil characterization.

pH	OM (%)	NO3-N(ppm)	P (ppm)	K (ppm)	NH4-N (ppm)	Ca (ppm)	Mg (ppm)	(Na (ppm)	CEC	S (ppm)	Sand (%)	Silt (%)	Clay (%)
8.0	1.8	12.5	44	197	14	2640	66	12	14	12	27	60	13